

Historical Climate Trends over High Mountain Asia Derived from ERA5 Reanalysis Data

S. KHANAL,^{a,b} S. TIWARI,^{b,c} A. F. LUTZ,^{b,d} B. V. D. HURK,^{a,e} AND W. W. IMMERZEEL^d

^a *Vrije University, Institute for Environmental Research, De Boelelaan, Amsterdam, Netherlands*

^b *FutureWater, Costerweg, Wageningen, Netherlands*

^c *Department of Hydrology and Quantitative Water Management Group, Wageningen University, Wageningen, Netherlands*

^d *Department of Physical Geography, Utrecht University, Utrecht, Netherlands*

^e *Deltares, Boussinesqweg, Delft, Netherlands*

(Manuscript received 23 March 2021, in final form 18 October 2022)

ABSTRACT: The climate of High Mountain Asia (HMA) has changed in recent decades. While the temperature is consistently increasing at a higher rate than the global warming rate, precipitation changes are inconsistent, with substantial temporal and spatial variation. Climate warming will have enormous consequences for hydroclimatic extremes. For the higher altitudes of the HMA, which are a significant source of water for the large rivers in Asia, often trends are calculated using a limited number of in situ observations mainly observed in valleys. This study explores the changes in mean, extreme, and compound-extreme climate variables and their seasonality along the full altitudinal range in HMA using daily ERA5 reanalysis data (1979–2018). Our results show that winter warming and summer wetting dominate the interior part of HMA. The results indicate a coherent significant increasing trend in the occurrence of heatwaves across all regions in HMA. The number of days with heavy precipitation shows more significant trends in southern and eastern basins than in other areas of HMA. The dry period occurrence shows a distinct demarcation between lower- and higher-altitude regions and is increasing for most basins. Although precipitation and temperature show variable tendencies, their compound occurrence is coherent in the monsoon-dominated basins. These changes in indicators of climatic extremes may imply substantial increases in the future occurrence of hazards such as floods, landslides, and droughts, which in turn impact economic production and infrastructure.

KEYWORDS: Asia; Complex terrain; Climatology; Risk assessment; Reanalysis data; Trends


1. Introduction

High Mountain Asia (HMA) serves as a major water source for large rivers in Asia (Immerzeel and Bierkens 2012). HMA consists of the Tibetan Plateau (TP), surrounded by the mountain ranges of Tien Shan, Pamir, Hindu Kush, and the Karakoram in the west, the Himalayas in the south and southeast, and Qilian Shan in the east. Over 1.4 billion people in various countries, including Afghanistan, Bangladesh, Bhutan, China, India, Kazakhstan, Kyrgyzstan, Mongolia, Myanmar, Nepal, Pakistan, and Tajikistan, depend on water originating from HMA. The topography and atmospheric circulation patterns mainly define the region's climate variability (MauSSION et al. 2014; Schiemann et al. 2009; Webster et al. 1998). The region has strong longitudinal (west–east), latitudinal (north–south), and vertical climate gradients (Yao et al. 2012). The climate of HMA is driven by the interaction of the Indian summer monsoon, dominant in the south-eastern parts, while winter westerly winds dominate the climate in the western region. The steep north–south orography results in strong temperature gradients that drive the moisture-laden winds from the Indian Ocean to the landmass,

and ultimately the moisture is released under the orographic influence.

Consequently, the southern and eastern parts of HMA receive nearly 80% of the yearly precipitation from June to September during the monsoon season, which occurs as rainfall at low altitudes and snow at high altitudes (Bookhagen and Burbank 2010). Conversely, the westerly winds in the west, originating from the Mediterranean, contribute around 50% of annual precipitation during winters, mainly falling as snow (Bao and You 2019; Rees and Collins 2006). The interaction of the monsoon and westerlies, where the monsoon has a dominant role in the summer months and westerlies in the winter months, influences the climate of the interior TP (Frauenfeld et al. 2005; Yang et al. 2014; You et al. 2015b).

The climate of HMA has witnessed many changes in recent decades. There are spatially consistent and statistically significant warming trends over the different regions of HMA (Krishnan et al. 2019; Liu and Chen 2000). Studies based on ground-based observations have consistently reported warming trends over the TP in the past (Kosaka and Xie 2013; Liu and Chen 2000; Yan and Liu 2014). Tien Shan, Central Asia, and the Hindu Kush Himalayas (HKH) region have observed

 Denotes content that is immediately available upon publication as open access.

Corresponding author: Sonu Khanal, s.khanal@futurewater.nl



This article is licensed under a [Creative Commons Attribution 4.0 license](http://creativecommons.org/licenses/by/4.0/) (<http://creativecommons.org/licenses/by/4.0/>).

DOI: 10.1175/JAMC-D-21-0045.1

© 2023 American Meteorological Society. For information regarding reuse of this content and general copyright information, consult the [AMS Copyright Policy](https://www.ametsoc.org/PUBSReuseLicenses) (www.ametsoc.org/PUBSReuseLicenses).

similar warming trends (Aizen et al. 1997; Hu et al. 2014; Ren et al. 2017). In contrast to temperature, precipitation shows a more considerable interannual variability, and inconsistency in trends for different regions in HMA (Fowler and Archer 2006; Palazzi et al. 2013; Ren et al. 2017; Shrestha et al. 2000; You et al. 2015b; Zhan et al. 2017). The climate variability in recent decades has resulted in changes in the cryosphere (glaciers, snow cover, and permafrost) and hydrology (water availability, seasonality, and hydrological extremes like floods and droughts), which in turn affect society (Bolch et al. 2012; Immerzeel et al. 2010; Jin et al. 2020; Kääb et al. 2012; Kang et al. 2010; Shean et al. 2020; Wijngaard et al. 2017; Yang et al. 2010; Yao et al. 2012).

Past studies used monthly-scale station data to derive the historical trends for different regions in HMA (Cao et al. 2013, 2017; Duan and Xiao 2015; Guo and Wang 2012; Khattak et al. 2011; Liu and Chen 2000; Shrestha et al. 1999, 2000; Xu et al. 2018; Yan and Liu 2014; Yang et al. 2014). Attempts were made with remote sensing techniques to calculate trends (Qin et al. 2009; Salama et al. 2012; Zhong et al. 2011). Some recent studies used the general circulation model data downscaled with fine-resolution regional climate models to calculate the long-term trends (Amato et al. 2019; Zhang et al. 2017). Moreover, some studies combined in situ and reanalysis data to understand the spatial pattern of historical climate change (An et al. 2017; Krishnan et al. 2019; Madhura et al. 2015). However, these studies are either scattered around the basin, national and regional levels. Further, these scattered studies use different data, coarser spatiotemporal resolution, and approaches. Variability in approaches, data, and methods makes it even more challenging to align and compare the changes around different regions in HMA. Studies that use consistent, observed, and remotely sensed data integrated with numerical models at a higher spatial resolution over the entire HMA region are required to resolve the climate variability in the region.

Existing hydrometeorological stations, mostly located in valleys lower than 4000 m, are sparsely distributed in the region (Pepin et al. 2015; Qin et al. 2009). The complex topography and harsh conditions in the mountains impose difficulties in managing the ground stations. Therefore, climate signals are biased toward these station observations at lower elevations (An et al. 2017; Palazzi et al. 2013). Remotely sensed satellite measurements from geostationary thermal infrared and polar-orbiting passive microwave sensors are useful for deriving precipitation measurements based on cloud-top brightness temperature and spectral scattering due to large ice particles, respectively. However, the uncertainty is high due to sensor signals' limitations in penetrating the clouds and correctly estimating the precipitation falling as snow at high altitudes (Immerzeel et al. 2015). Nevertheless, remotely sensed products or products merged with gauge observations, in recent decades, have proven to be a cost-effective and reliable tool to understand precipitation patterns and trends at various spatial and temporal scales (Gehne et al. 2016). Among other remotely sensed products (or merged products), the Tropical Rainfall Measuring Mission (TRMM), the Climate Hazard group Infrared Precipitation (CHIRPS), the Multi-Source Weighted-Ensemble Precipitation (MSWEP),

the Climate Prediction Center morphing technique (CMORPH) and the Precipitation Estimation from Remotely Sensed Information using Artificial Neural Network (PERSIANN) and are most commonly used in the HMA region for a wide range of applications (Ashouri et al. 2015; Beck et al. 2017; Funk et al. 2015; Huffman et al. 2007; Joyce et al. 2004; Yatagai et al. 2012). The direct use of such products to derive climatological and hydrological trends often requires validation and correction based on in situ observations (Gebregiorgis and Hossain 2015; Gehne et al. 2016). The correction is often hampered by the mismatch in resolution and insufficient geo-statistical interpolation accuracy of in situ data caused due to sparse gauge distribution. Moreover, these global remotely sensed (or merged with gauge observation) products have higher uncertainty in assessing the correct precipitation amount in an environment with complex mountainous topography such as HMA (Cheema and Bastiaanssen 2012; Mei et al. 2014). A common scientific consensus, based on a plethora of studies, could be made that all these remotely sensed (or products merged with gauge observation) products have large and variable biases relative to the gauge data in HMA (Andermann et al. 2011; Cheema and Bastiaanssen 2012; Guo et al. 2015; Tong et al. 2014; You et al. 2015a).

A gridded reanalysis product—which is a result of data assimilation from multiple sources: airborne balloons, scatterometer radiosonde, dropsonde, aircraft measurements, satellites, and ground-based radar-gauge composite—provides an alternative to the sparse and inconsistent point-scale observations to find spatial patterns of change (Alexander et al. 2006; Li et al. 2022). Even though biases between reanalysis and in situ observations are present, the reanalysis products have shown good reliability in resolving the climatological mean, anomalies, and normalized trends (Donat et al. 2014; Simmons et al. 2010). Given the high variability in the climate of HMA, this paper aims to assess trends in annual and seasonal air temperature and precipitation and a range of climate change indices for the high-altitude regions. We use the state-of-the-art ERA5 high-resolution reanalysis data to derive the trends (Hersbach et al. 2020). These trends help us to detect similarities and contrasts in recent climate change over the entire HMA using one consistent dataset.

2. Study area

The HMA, consisting of the TP and its surrounding high mountain ranges along with its 18 downstream river basins, is considered for this study (Fig. 1a). Within this region, the Hindu Kush Himalayan (HKH) range along with the TP covers an area of over 5 million km² with an average elevation of ~4000 m above mean sea level (MSL) (Yao et al. 2012). The areal extent considered in this study is 57°–113°E and 22°–47°N. Given the large extent of the study area, the overall climate is variable. For example, in the west, the Helmand, Amu Darya, and Syr Darya River basins have a dry continental climate characterized by cold winters and hot summers (Chen et al. 2011), while in the east, the Yangtze basin has a subtropical climate with maximum rain between April and

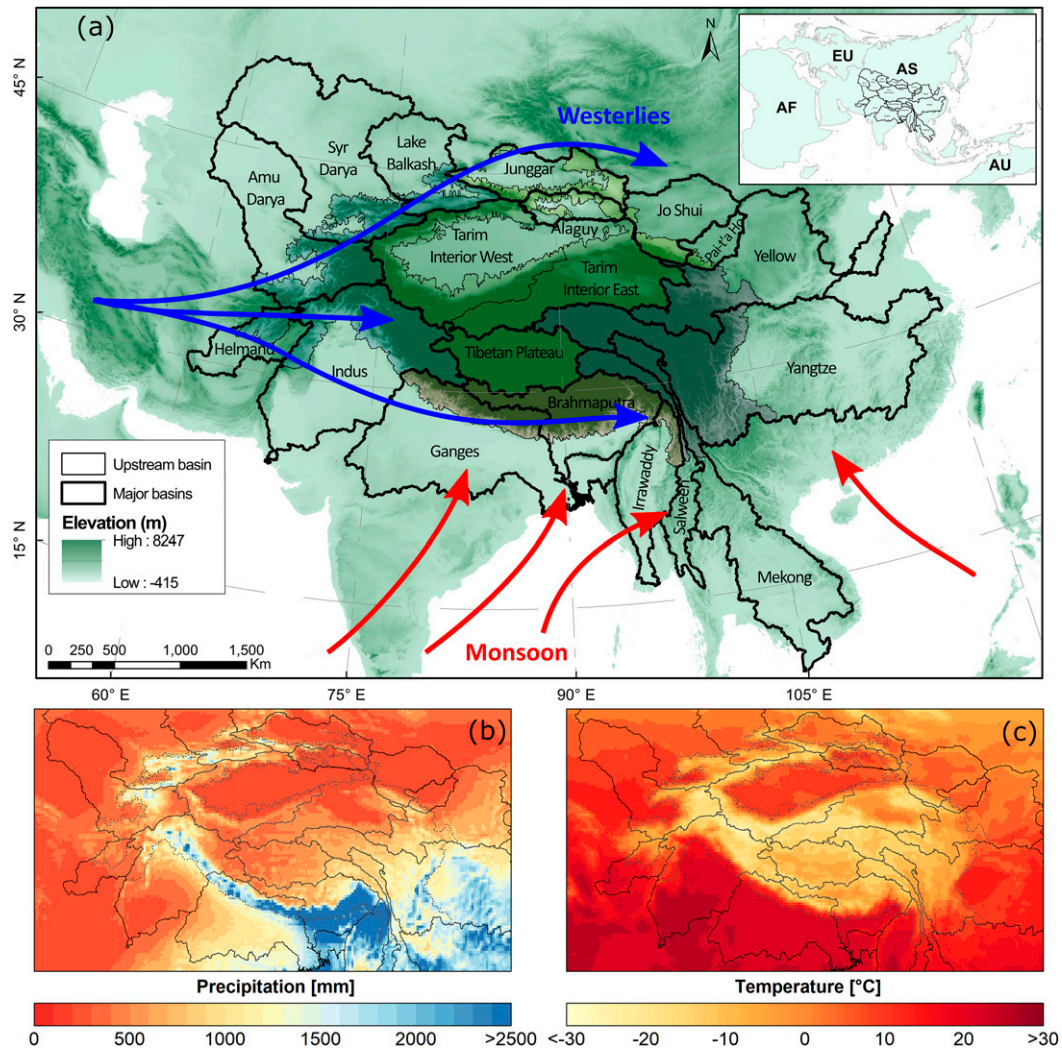


FIG. 1. (a) The river basins analyzed in this study (black boundaries). Gray lines represent the upstream region of each major river basin. The background represents the elevation of the region. The arrows represent the major atmospheric circulation system, red for monsoon and blue for westerlies, in HMA [the arrows are adapted from [Yang et al. \(2014\)](#)]. Also shown is the spatial distribution of mean annual (b) precipitation (mm) and (c) temperature (°C) during 1979–2018 across HMA.

October ([Gu et al. 2018](#)). The northwestern basins, Balkash, Junggar, and Alaguy are influenced mainly by midlatitude westerlies and cold inflows from the polar region. The TP, generally below 0°C and temperature decreasing from east to west, experiences cold winters and wet summers, with maximum precipitation during July and August ([Frauenfeld et al. 2005](#)). Climatic differences enhance the spatial variation within each basin's higher and lower altitudes ([Krishnan et al. 2019](#); [You et al. 2017](#)). A significant part of the southeastern basin's precipitation is from the southwestern Indian monsoon between June and September. The winter monsoon brings rain to the northwestern part of the HKH. At high altitudes, precipitation mainly falls as snow, whereas at lower altitudes it mainly falls as rain. The Central Asian basins receive annual precipitation of ~211 mm, ranging from less

than 50 mm in the desert areas to higher than 2000 mm on the windward slopes ([Deng and Chen 2017](#)).

3. Data and methods

We use historical climate data from the European Centre for Medium-Range Weather Forecasts (ECMWF) ERA5 dataset covering the years 1979–2018 (40 years) ([Hersbach et al. 2020](#)). The ERA5 is an improved (atmosphere, ozone, land, and ocean wave component) and high-resolution successor of the ERA-Interim ([Dee et al. 2011](#)). The ERA5 uses observations from over 200 satellite instruments or conventional data types, including ground-based radar–gauge observations, PILOT, radiosonde, dropsonde, buoys, and aircraft measurements. The ERA5 data are available at an hourly time scale

TABLE 1. Summary of the findings related to ERA5 data reported in several studies.

Study	Regions	Products	Variable	Findings
Orsolini et al. (2019)	Tibetan Plateau	4 products (reanalysis)	Snow depth and cover; precipitation	Excessive snowfall results in overestimation of snow depth and cover; cold bias
Bian et al. (2019)	Tibetan Plateau	12 products (observation, satellite estimate, land data assimilation system, and reanalysis)	Snow water equivalent; temperature; total precipitation; snowfall	Significant overestimates the SWE; cold bias
Zandler et al. (2019)	Pamir region of Tajikistan	10 products (satellite, gridded, merged, and reanalysis)	Precipitation	Significant performance improvement in ERA5 relative to others
Tang et al. (2020)	China	10 (7 satellite and 3 reanalysis)	Precipitation; snowfall	Acceptable at the daily-scale use; performs best relative to the reanalysis products; peak time, magnitude, and variation of diurnal cycles not well represented
Ji and Yuan (2020)	Tibetan Plateau	8 products (2 land data assimilation system, 5 reanalysis, and a high-resolution dynamical downscaling simulation)	Temperature (min, max, and mean)	Cold bias in ERA5
Jiang et al. (2020)	China	5 (satellite-based precipitation)	Precipitation	Correct precipitation distribution; performs best in detecting typhoon induced extreme precipitation events; underestimates moderate and higher daily precipitation events (above 10 mm day ⁻¹)
Dahri et al. (2021b)	Upper Indus	27 (gridded precipitation products)	Precipitation	Best performance
Hu and Yuan (2021)	Eastern periphery of the Tibetan Plateau	82 ground stations	Precipitation	Captures the spatiotemporal features of the regional rainfall events; higher frequency and lower intensity of rainfall events; incorrect timings of precipitation events
Sun et al. (2021)	High Mountain Asia	584 ground station	Precipitation; discharge	Performs better in the monsoon-dominated regions than westerlies-dominated regions; represents large-scale spatial precipitation pattern; precipitation estimates can detect well the monsoon and westerlies signal; wetter in central and western HMA and drier in the southeast; captures precipitation seasonality of Tarim basin, which is not reflected from GPM and outputs of regional climate model
Lei et al. (2022)	China	666 ground stations	Precipitation	Correctly simulates annual total precipitation; correctly estimates intensity indices such as annual total wet days precipitation, max 5-day precipitation, very wet days, max 1-day precipitation amount and extremely wet days; better at simulating drought events than wet events over eastern China; underestimates number of extreme heavy precipitation days

and 31 km × 31 km spatial resolution for 137 vertical pressure levels. Surface or single-level data are also available, containing two-dimensional parameters such as precipitation, 2 m temperature, top-of-atmosphere radiation, and vertical integrals over the entire atmosphere.

The utility of ERA5 in complex terrain such as HMA, where the in situ meteorological observations are sparsely and unevenly distributed, has been investigated in several

studies (see Table 1). ERA5 has been validated in several regions of the HMA, for instance, the Pamir region of Tajikistan (Zandler et al. 2019), the Indus basin (Dahri et al. 2021b), mainland China (Jiang et al. 2020; Lei et al. 2022; Tang et al. 2020), Tibetan Plateau (Hu and Yuan 2021; Ji and Yuan 2020), and HMA (Sun et al. 2021). The study by Lei et al. (2022), on the basis of 666 ground stations over China, showed that annual total precipitation was correctly simulated

TABLE 2. List of climate indices used in this study.

Indicator	Definition	Unit	Related hazards
Consecutive dry days (CDD)	The largest No. of consecutive days with <1 mm of precipitation	Days	Drought
Heatwave duration index (HWDI)	No. of days, in intervals of at least 6 consecutive days, when the max temperature is more than 5° larger than the normal max temperature (TXnorm); TXnorm is calculated as the mean of max temperatures of a 5-day window centered on each calendar day of a given climate reference period	Days	Drought
R10	No. of heavy precipitation days (precipitation > 10 mm)	Days	Floods
RX5	Annual highest 5-day precipitation sum	mm	Floods
R95P	Wet days precipitation (precipitation > 1 mm) when daily precipitation is greater than 95th percentile of all wet days	mm	Floods
COMP95	The No. of days when both precipitation and temperature are greater than the 95th percentile of their distribution considering all days	Days	Floods

when compared with the daily total in ERA5. Authors suggested ERA5 performs well for simulating intensity indices such as annual total wet days precipitation, max 5-day precipitation, very wet days, max 1-day precipitation amount and extremely wet days. Frequency indices such as extreme heavy precipitation days were consistently well simulated across China except northwestern China in ERA5. ERA5 better simulated the consecutive dry days than the consecutive wet days. Similarly, [Sun et al. \(2021\)](#) found that ERA5 precipitation generally captures the seasonal variations of ground observations (monsoon and westerlies patterns) and the broad spatial distributions of precipitation in both magnitude and trends in HMA. Interestingly, ERA5 well represents the precipitation seasonality of the Tarim basin, which is not reflected in GPM and outputs from the regional climate model. Moreover, ERA5 data have been used to understand the precipitation and large-scale atmospheric systems ([Lai et al. 2021](#); [Wang et al. 2020](#); [Yu et al. 2021](#); [Zhu et al. 2020](#)), snow cover and snow depth ([Lei et al. 2023](#)), glacier and snowmelt simulation ([Bhattacharya et al. 2021](#); [Kraaijenbrink et al. 2021](#)), and hydrological and water balance simulations ([Dahri et al. 2021a](#); [Khanal et al. 2021](#); [Sun et al. 2021](#)).

We further assess the performance of six different gauge-based gridded precipitation products (CHIRPS, TRMM, PERSIANN, GLDAS, CFSV2, and GPM) and compared them with ERA5 over the HMA ([Fig. A1](#) in the [appendix](#)). The average annual precipitation patterns show more or less similar large-scale spatial patterns. ERA5 seems to be wetter in the southern and eastern parts relative to the other regions of HMA. The differences are also noticeable in region-aggregated climatological analysis. CFSV2 seems to be on the drier side for the monsoon period where as the GLDAS is drier for the dry seasons. In general, ERA5 overestimates the precipitation in comparison with the six products. Satellite-derived products are of insufficient quality to capture the magnitude of mountain precipitation ([Immerzeel et al. 2015](#)). Authors found that the amount of precipitation required to sustain the observed mass balances of the large glacier systems in the Indus basin is far (by a factor of 5–10) beyond what is observed at valley stations or estimated by gridded precipitation products.

There is no perfect product in HMA as the ground-based observations at upper altitudes of HMA are lacking ([Sun et al. 2021](#)). Precipitation products are not equally good enough for all the basins in HMA. Even though ERA5 overestimates the precipitation in comparison with the other products (satellite, gridded, reanalysis, and model simulation), the aforementioned studies show that the ERA5 has a wide range of utility. ERA5 captures the seasonal variations of ground observations and the broad spatial distributions of precipitation in both magnitude and trends when it comes to data-scarce upstream regions of HMA. Thus, we conclude that ERA5 is good enough to use to understand the climatic trends in HMA.

The daily aggregated surface level precipitation sum and mean temperature are used in this study to derive historical climate indicators as described in [Table 2](#). We analyze each climate indicator on an annual scale and seasonal scale: (i) winter [December, January, and February (DJF)], (ii) summer or premonsoon [March, April, and May (MAM)], (iii) monsoon or rainy [June, July, August, and September (JJAS)], and (iv) post-monsoon or autumn [October and November (ON)].

The climate indicators analyzed for this study are consecutive dry days (CDD), heatwave duration index (HWDI), highest 5-day precipitation amount (RX5), heavy precipitation days (R10), wet days precipitation (R95P), and compound indices (COMP95). The first five indices used are defined and described in [Zhang et al. \(2011\)](#). We define COMP95 as the number of days when both precipitation and temperature are greater than the 95th quantile values of their distributions. The COMP95 is used as a proxy for floods because it indicates the “Warm-Wet” quadrant of the precipitation and temperature distribution. A similar approach is used in [Khanal et al. \(2021\)](#) and [Lutz et al. \(2016\)](#). For convenience, we use CDD and HWDI as the proxy for droughts and their related hazards, and R10, RX5, R95P, and COMP95 as a proxy for flood-related hazards. The relationships between the climate indices and floods/droughts are often complex. Changes in the trend of these indicators may not directly lead to floods or droughts. However, they would certainly lead to changes in the antecedent conditions and state of the precursors (saturation content

TABLE 3. Average basin and climatic characteristics calculated for the upstream parts of the major river basins. The climate of the basin can be of monsoon or westerly or mixed type. The upstream area represents the percent of major river basins used as the upstream part in this study. The numbers inside the parentheses represent the trend, and boldface numbers represent a significant trend at the $p < 0.05$ level.

Basin	Region	Climate	Mean elev (m MSL)	Area (km ²)	Upstream area (%)	Mean precipitation (mm)	Mean temperature (°C)
Brahmaputra	Southern	Monsoon	4003	400	75.7	1978 (−2.25)	1.7 (0.03)
Ganges	Southern	Monsoon	3090	202	17.8	1755 (5.03)	6.8 (0.03)
Irrawaddy	Southern	Monsoon	2109	49	12.6	3593 (− 24.73)	12.9 (0.02)
Mekong	Eastern	Monsoon	3968	111	13.7	1035 (−1.37)	0.8 (0.03)
Salween	Eastern	Monsoon	4430	119	44.4	1096 (−2.31)	−2.1 (0.04)
Yangtze	Eastern	Monsoon	3678	687	38.5	1108 (−0.13)	1.9 (0.03)
Yellow	Eastern	Monsoon	3389	273	31.8	740 (−0.06)	0.5 (0.04)
Amu Darya	Western	Westerly	2930	268	33.6	678 (−1.29)	0.8 (0.03)
Balkash	Western	Westerly	2144	121	27.2	877 (−0.28)	1.2 (0.02)
Helmand	Western	Westerly	2355	74	29.7	367 (−2.11)	9.8 (0.05)
Indus	Western	Westerly	3511	473	42.4	837 (−1.98)	0.6 (0.04)
Syr Darya	Western	Westerly	2331	173	15.5	941 (1.10)	2.5 (0.03)
Alaguy	Northern	Westerly	1506	75	51.8	218 (−0.47)	6.8 (0.03)
Pai-t'a Ho	Northern	Westerly	2664	16	14.4	633 (−1.07)	0.6 (0.05)
Jo-Shui	Northern	Westerly	2575	66	18.8	395 (0.57)	1.3 (0.05)
Junggar	Northern	Westerly	1778	152	44.9	387 (−0.18)	3.0 (0.02)
Plateau of Tibet Interior	Interior	Mixed	4996	415	100	444 (3.57)	−3.2 (0.03)
Tarim Interior East	Interior	Mixed	3842	600	37.8	305 (1.63)	−2.4 (0.04)
Tarim Interior West	Interior	Mixed	3301	481	30.3	371 (0.14)	−0.9 (0.03)

of the soil, groundwater state, rain on snow, etc.) related to floods and droughts (Merz et al. 2014; Nied et al. 2014). For instance, the increasing trend in R10 and RX5 would mean higher episodes of precipitation events that may impact the soil moisture conditions. Any medium to high precipitation episode on saturated soil most likely results in floods (Khanal et al. 2019; Merz et al. 2014; Nied et al. 2014). We also calculate the standardized precipitation anomaly (SPA) and standardized temperature anomaly (STA) on a regional scale to understand the regional patterns of floods and droughts.

We calculate the magnitude of the trend for each index using the Theil–Sen slope estimate, and its significance at 5% ($p < 0.05$) using the nonparametric Mann–Kendall's significance test (Mann 1945; Sen 1968). It is preferred over other parametric tests since the data do not need to be normally distributed or homogeneous, and the effect of outliers is reduced as it is based on median values rather than means (Gilbert 1987). The Theil–Sen slope method involves calculating the slope Q and its median for each data point in time to calculate the trend. The slope for each data point is calculated as

$$Q = \frac{x'_i - x_i}{i' - i}, \quad (1)$$

where x'_i and x_i are data values at times i' and i , respectively, and $i' > i$. The median of Q represents the Theil–Sen trend. Before trend analysis, the data were checked for autocorrelation and corrected based on Yue and Wang (2002). We focus our analysis on the high-altitude upstream parts of each river basin. The upstream region used in this study is defined as all areas above 2000 m, as used by Khanal et al. (2021), and is

delineated using the HydroSHEDS digital elevation model (Lehner et al. 2008). Further, we categorize river basins in HMA by climatic regions (Table 3). Since the Tarim basin exhibits different climatic characteristics, we make a further distinction between the Tarim interior East (TIE) and the Tarim interior West (TIW). Unless specified, the Tarim basin represents the whole of TIW and TIE. All the results presented in this study will represent the upper or upstream region unless specified explicitly. The basin average trends are calculated for the area aggregated basin average time series.

4. Results

a. Climatic characteristics

The HMA region shows considerable variability in climatic characteristics, as shown in Table 3. The monsoon-dominated southern river basins generally receive the highest amounts of precipitation (Fig. 1b). The Irrawaddy (3593 mm), Brahmaputra (1978 mm), and Ganges (1755 mm) basins are the wettest basins, whereas the Alaguy (218 mm) and Helmand (367) are the driest basins in HMA. The steep elevation gradient along the north–south and the monsoon are the main reasons that the southern basins receive most orographic precipitation. The average temperature in the region shows a distinct difference between the high-altitude colder mountainous regions and the warmer plains (Fig. 1b). The northern basins are the coldest of the whole HMA. The relatively cold temperature is mainly due to a higher mean elevation than other basins in HMA (Table 3). The monsoon-dominated downstream areas of the Ganges, Indus, Irrawaddy, and Salween basins show the highest temperature. These regions are known

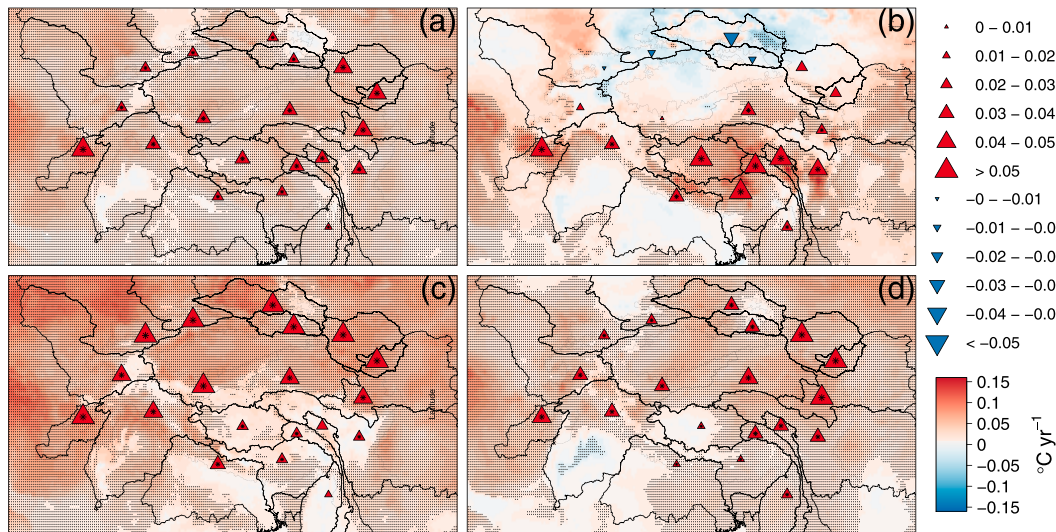


FIG. 2. (a) Average daily mean temperature over the entire TP during 1979–2018, and (b) winter, (c) summer, and (d) monsoon trends of mean temperature ($^{\circ}\text{C yr}^{-1}$) estimated using Sen's slope. Stippling represents areas with Kendall's significance at $p < 0.05$. The triangles, red upward for an increase and blue downward for a decrease, represent the upper-basin-averaged temperature trends. The presence of a black asterisk in the triangle indicates areas with Kendall's significance at $p < 0.05$ for upper-basin-averaged temperature trends.

to experience warm summers with extreme heat events and cold winters (Im et al. 2017). Given the large extent of the study area, the overall climate is variable.

b. Trends in temperature and temperature-derived indices

1) MEAN AIR TEMPERATURE

The annual temperature trends are coherent and statistically significant over the entire region (Fig. 2a; Table 4). The cooling of irrigated Indo-Gangetic plains is in line with the

finding that an increase in irrigated areas can lower the magnitude of climate change and extremes (Puma and Cook 2010; Thiery et al. 2017). The averaged annual trend ($0.05^{\circ}\text{C yr}^{-1}$ to $2.12^{\circ}\text{C yr}^{-1}$ over 40 years) in the Helmand basin is in line with 2.2°C increase reported by Krishnan et al. (2019) (Fig. 2a; Table 3). The annual warming of regions in HMA is higher relative to the Northern Hemisphere ($0.024^{\circ}\text{C yr}^{-1}$ for land and oceans and $0.033^{\circ}\text{C yr}^{-1}$ for land) and the global average ($0.017^{\circ}\text{C yr}^{-1}$ for land and oceans and $0.03^{\circ}\text{C yr}^{-1}$ for land) calculated for time 1979–2018 using Global Historical Climatology Network

TABLE 4. Average temperature ($^{\circ}\text{C}$) for the reference time period (1979–2018) selected for the analysis. The numbers inside the parentheses represent the trend ($^{\circ}\text{C yr}^{-1}$), and boldface numbers represent the significance of trend at $p < 0.05$ level.

Basin	Annual	DJF	MAM	JJAS	ON
Brahmaputra	1.7 (0.029)	−7.3 (0.054)	1.0 (0.022)	9.7 (0.020)	−0.2 (0.027)
Ganges	6.8 (0.029)	−1.6 (0.038)	6.5 (0.031)	13.9 (0.019)	5.4 (0.03)
Irrawaddy	12.9 (0.018)	6.3 (0.022)	13.0 (0.010)	18.0 (0.021)	12.3 (0.014)
Mekong	0.8 (0.034)	−9.3 (0.063)	0.4 (0.024)	10.1 (0.03)	−2.3 (0.027)
Salween	−2.1 (0.035)	−12.7 (0.052)	−2.9 (0.023)	8.0 (0.030)	−5.4 (0.022)
Yangtze	1.9 (0.033)	−7.8 (0.042)	1.9 (0.021)	10.4 (0.037)	−0.8 (0.024)
Yellow	0.5 (0.042)	−10.9 (0.025)	0.9 (0.046)	10.3 (0.053)	−2.8 (0.037)
Amu Darya	0.8 (0.029)	−10.9 (0.011)	0.4 (0.042)	11.3 (0.038)	−2.2 (0.026)
Lake Balkash	1.2 (0.022)	−11.3 (−0.019)	2.0 (0.055)	11.6 (0.027)	−2.1 (0.017)
Helmand	9.8 (0.053)	−3.7 (0.063)	9.1 (0.073)	21.2 (0.043)	8.2 (0.027)
Indus	0.6 (0.036)	−10.7 (0.034)	−0.4 (0.046)	11.1 (0.033)	−1.9 (0.052)
Syr Darya	2.5 (0.026)	−9.7 (−0.005)	2.9 (0.058)	12.8 (0.028)	−0.9 (0.016)
Alaguy	6.8 (0.027)	−9.1 (−0.014)	8.7 (0.054)	19.7 (0.039)	1.9 (0.03)
Pai-t'a Ho	0.6 (0.049)	−12.3 (0.029)	1.2 (0.073)	11.4 (0.056)	−3.1 (0.034)
Jo-Shui	1.3 (0.046)	−12.1 (0.024)	2.0 (0.068)	12.6 (0.054)	−2.9 (0.035)
Junggar	3.0 (0.020)	−12.7 (−0.030)	4.3 (0.059)	15.8 (0.035)	−1.6 (0.021)
Plateau of Tibet Interior	−3.2 (0.033)	−13.3 (0.053)	−3.6 (0.024)	6.2 (0.018)	−6.5 (0.036)
Tarim Interior East	−2.4 (0.039)	−14.0 (0.030)	−2.2 (0.045)	8.0 (0.046)	−6.4 (0.026)
Tarim Interior West	−0.9 (0.034)	−13.3 (0.001)	−0.3 (0.052)	9.6 (0.037)	−4.7 (0.037)

(NOAA 2020). The seasonal spatial trends show that the increase ($0.08^{\circ}\text{--}0.10^{\circ}\text{C yr}^{-1}$, or $3.2^{\circ}\text{--}4.0^{\circ}\text{C}$ over 40 years) is most apparent in the headwaters of the southern, monsoon-dominated basins of the Ganges, the Brahmaputra, and the interior basins in winter (Fig. 2b). The winter warming trend is higher for eastern TP, for which an increase of $0.61^{\circ}\text{C decade}^{-1}$ ($\sim 2.44^{\circ}\text{C}$ over 1961–2006) is reported (Liu et al. 2009). Strikingly, the northern basins, Junggar, Alagay, and Balkash show a decreasing winter temperature trend. Several studies report a similar winter cooling in the Northern Hemisphere and attribute it to the increase in Eurasian snow cover contributed by the warmer moisture-laden arctic atmosphere in the autumn season (Cohen et al. 2014, 2020, 2012). A relatively smaller warming trend is observed in the monsoon season when compared with the summer and winter seasons (Figs. 2b–d). The irrigated downstream region of the Indus shows a significant decrease in temperatures during the monsoon season, implying that most of the annual decline in temperature trend is contributed by the monsoon season.

2) HEATWAVE DURATION INDEX

The annual average HWDI is relatively low in most parts of the study region except the lower regions of the westerly dominated basin (Fig. 3; Table 5). We find high HWDI “hotspots” in the southern and eastern monsoon-dominated basins of the Brahmaputra, Ganges, Salween, the Mekong, and the Yangtze. We further investigate the annual anomalies of HWDI for two different climatic regions, the westerly-dominated Helmand basin and the monsoon-dominated Salween basin, to understand these high HWDI “hotspots” (Figs. 3b,c). We found the maximum HWDI in the Salween basin in 2016 correlates with the century’s strongest El Niño event (Cai et al. 2018). The spatial annual HWDI trend, in general, does not show significant changes in HMA apart from the lower regions of western and eastern basins (Fig. 3d). Interestingly, the smaller “hotspots” in the Salween and the Mekong do not show a consistent trend, indicating that the high values are reached due to large-scale climate events such as the El Niño that are known to influence the climate of the Indian Subcontinent (Krishnan et al. 2019). Again, the upper-basin-averaged annual HWDI trend shows minimal changes with the maximum increase seen in Helmand, $0.44 \text{ days yr}^{-1}$, and for most regions, the values range between 0.1 and 0.2 days yr^{-1} (Fig. 3d).

c. Trends in precipitation and precipitation-derived indices

1) ANNUAL PRECIPITATION

Even though annual precipitation shows a higher variability in HMA, the trends are only significant for four basins (Table 3). The western basins show a decreasing annual precipitation trend, except for the Syr Darya, where annual precipitation increases by $0\text{--}5 \text{ mm yr}^{-1}$ (Fig. 4a). In contrast to the western basins, the monsoon-dominated southern and interior basins show an increasing annual precipitation trend. Strikingly, the western and eastern regions of Brahmaputra show contradictory trends in annual precipitation. The western Brahmaputra shows a

significant increasing trend ($5\text{--}15 \text{ mm yr}^{-1}$), whereas the eastern part shows a significant decreasing annual precipitation trend ($50\text{--}70 \text{ mm yr}^{-1}$). The significant decreasing trends in regions such as the eastern Brahmaputra and upper Irrawaddy basin correlates with areas that receive the highest precipitation. The lower parts of eastern basins show statistically significant decreasing trends ($5\text{--}15 \text{ mm yr}^{-1}$) as compared with the increasing trends for upper regions. The relative precipitation increase is highest for the interior basin than for the other regions in HMA (Fig. 4b). The trends found in this study are in line with those reported by Cuó et al. (2013) based on in situ observations for the Northern TP. The upper-basin-averaged annual trend reflects the highest decreasing trend of $\sim 25 \text{ mm yr}^{-1}$ in the Irrawaddy. The west-to-east opposite pattern of precipitation trend in the entire upper Brahmaputra basin ultimately results in an overall decreasing trend of -2.2 mm yr^{-1} , where the strong negative trend in the east clearly dominates the western Brahmaputra trend (Table 3). The monsoon months strongly dictate the annual precipitation trends in HMA (Fig. 4c; Table 6).

2) HEAVY PRECIPITATION DAYS (R10)

The annual spatial R10 shows a higher variability in the upstream part of the southern and eastern basins relative to other regions (Fig. 5a). The Irrawaddy, Brahmaputra, and Ganges show the highest annual R10 (112.3, 55, and 51.2 days, respectively) in the entire HMA (Table 7). The northern and interior basins have low R10 values when compared with the other basins. Higher variability and contradictory trend patterns within the basins are observed for the Brahmaputra and Ganges basins (Fig. 5b). Overall basin average R10 trend values in the Ganges ($0.1\text{--}0.2 \text{ days yr}^{-1}$) and Brahmaputra ($0\text{--}0.1 \text{ days yr}^{-1}$) basins show an increasing trend. Irrawaddy basin shows a spatially consistent decreasing trend similar to precipitation trends. The eastern basins show consistent decreasing trends except for the Yangtze basin. The lower Yangtze basin shows significantly decreasing trends than the middle reaches, where the trends are slightly positive. All western basins show coherent decreasing trends with the highest decrease in the western parts of Indus, except for the Syr Darya. Monsoon months contribute to most of the annual trends in the region (Fig. 5c). The monsoon trends are mostly coherent with the annual trends except in Helmand and the Syr Darya, where the sign of trends are reversed. The westerly precipitation regime is responsible for this reversal of trends.

3) ANNUAL MAXIMUM 5-DAY PRECIPITATION (RX5)

The southern basins show the highest RX5 day values in the entire HMA (Table 8). The foothills of the upper Ganges, Brahmaputra, and Irrawaddy basins receive higher RX5 than high altitudes (Fig. 6a). The low annual precipitation in the northern and interior basins is again reflected in annual RX5. The RX5 shows a decreasing annual trend, especially in the Brahmaputra and Irrawaddy basins (Fig. 6b). The weakening of the Indian summer monsoon is the primary reason for the decreasing RX5 trend in these basins. The upper Brahmaputra shows both significant spots of positive and negative trends; however, the latter is of a higher order of magnitude.

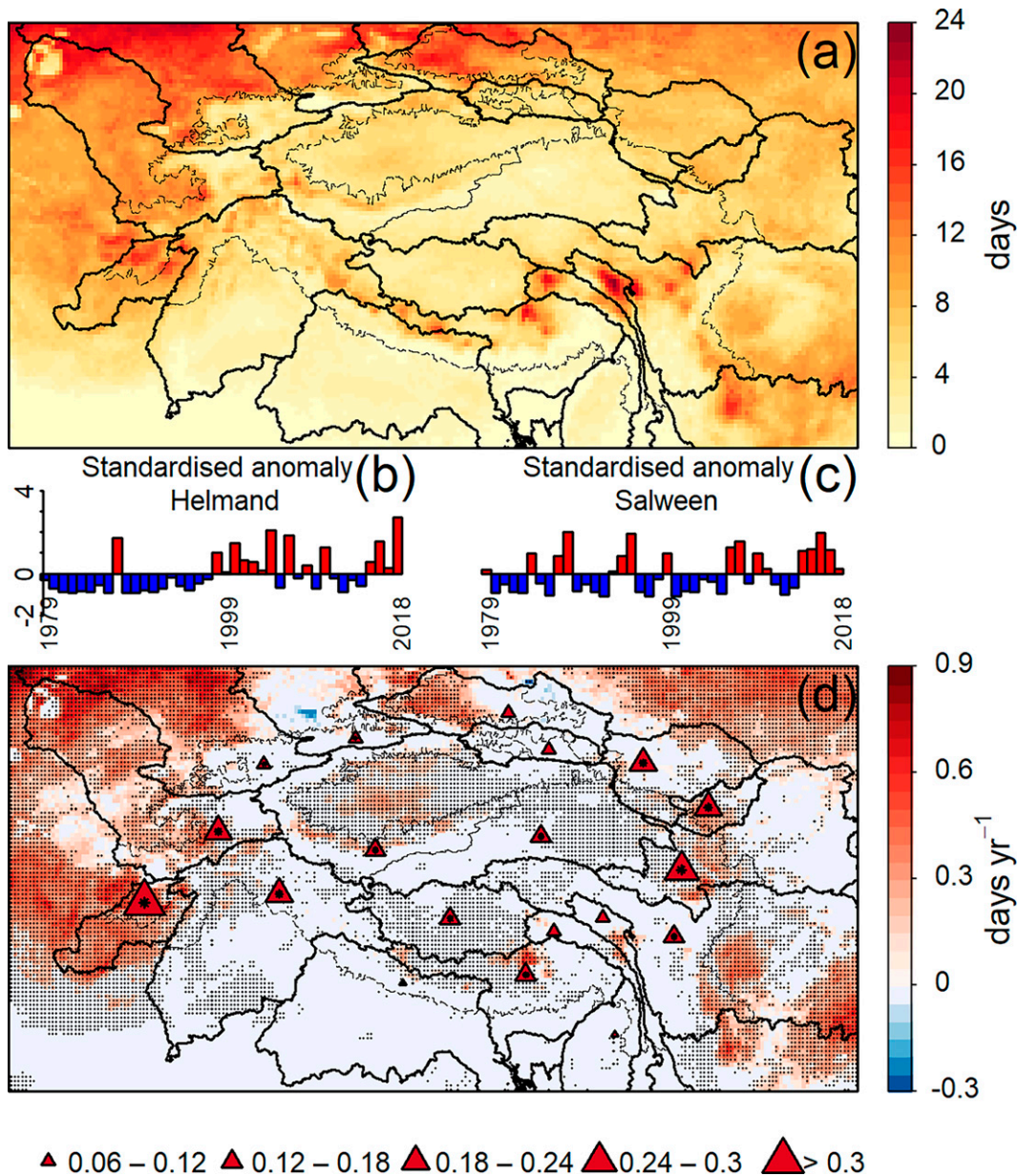


FIG. 3. (a) Average of annual HWDI over the entire HMA during 1979–2018 (days), standardized anomalies of annual HWDI for (b) the Helmand and (c) the Salween, and (d) annual HWDI trend (days yr⁻¹) estimated using Sen's slope. In (d), stippling represents areas with Kendall's significance at $p < 0.05$, the triangles, red upward for an increase and blue downward for a decrease, represent the upper-basin-averaged HWDI trends, and black asterisks denote areas with Kendall's significance at $p < 0.05$ for upper-basin-averaged HWDI trends.

In contrast, the Ganges basin shows an increasing trend for most of the upstream region.

The upper-basin-averaged RX5 shows mixed trends in the southern basins: the Irrawaddy and the Brahmaputra show negative trends whereas the Ganges basin shows positive trends. However, only in Irrawaddy, the trend (-1.8 mm yr^{-1}) is statistically significant at level $p < 0.05$. Among the eastern basins, a minor negative trend is observed for the Mekong, Salween, and Yangtze, and a positive trend is seen in the Yellow

River basin. Most of the annual trend in RX5 is contributed by the monsoon months' precipitation (Fig. 6c; Table 8). A similar pattern to annual trends is observed for monsoon months in entire HMA except for the western basins, where the winter and spring precipitation regimes are dominant.

4) WET DAYS PRECIPITATION (R95P)

A clear demarcation between the upper and lower basins, as seen in annual precipitation, R10, and RX5 is also detected

TABLE 5. Average HWDI (days) for the reference time period (1979–2018) selected for the analysis. The numbers inside the parentheses represent the trend (days yr⁻¹), and boldface numbers represent the significance of trend at $p < 0.05$ level.

Basin	Annual	DJF	MAM	JJAS	ON
Brahmaputra	4.4 (0.142)	2.7 (0.054)	0.7 (0.004)	0.1 (0.000)	0.7 (0.006)
Ganges	3.4 (0.057)	2.0 (0.018)	0.7 (0.000)	0.2 (0.000)	0.3 (0.000)
Irrawaddy	0.6 (0.000)	0.4 (0.000)	0.1 (0.000)	0.0 (0.000)	0.0 (0.000)
Mekong	8.0 (0.117)	3.3 (0.046)	1.3 (0.007)	0.4 (0.000)	2.7 (0.000)
Salween	6.9 (0.104)	2.9 (0.062)	1.2 (0.007)	0.4 (0.000)	2.2 (0.000)
Yangtze	5.4 (0.165)	2.4 (0.048)	1.1 (0.028)	0.5 (0.007)	1.0 (0.008)
Yellow	5.8 (0.240)	2.2 (0.075)	1.1 (0.031)	1.5 (0.051)	0.8 (0.000)
Amu Darya	7.2 (0.194)	2.7 (0.018)	1.9 (0.078)	0.4 (0.001)	1.9 (0.008)
Lake Balkash	5.4 (0.108)	1.4 (-0.018)	1.5 (0.021)	0.5 (0.000)	1.7 (0.004)
Helmand	12 (0.439)	7.0 (0.207)	4.2 (0.018)	0.0 (0.000)	0.3 (0.000)
Indus	6.2 (0.223)	2.3 (0.024)	1.6 (0.028)	0.6 (0.004)	1.4 (0.034)
Syr Darya	5.6 (0.119)	2.0 (0.014)	1.6 (0.035)	0.2 (0.000)	1.6 (0.000)
Alaguy	6.5 (0.103)	1.1 (0.000)	2.9 (0.020)	0.6 (0.000)	1.5 (0.000)
Pai-t'a Ho	6.8 (0.235)	2.2 (0.000)	2.3 (0.000)	1.2 (0.000)	0.8 (0.000)
Jo-Shui	5.9 (0.197)	2.0 (0.016)	2.2 (0.031)	0.7 (0.000)	0.8 (0.000)
Junggar	9.2 (0.095)	2.4 (-0.017)	3.1 (0.054)	0.9 (0.004)	2.1 (0.000)
Plateau of Tibet Interior	4.1 (0.129)	1.7 (0.006)	0.8 (0.002)	0.9 (0.000)	0.4 (0.001)
Tarim Interior East	3.1 (0.133)	1.0 (0.014)	0.8 (0.028)	0.8 (0.004)	0.3 (0.000)
Tarim Interior West	5.0 (0.142)	1.4 (0.002)	1.8 (0.043)	0.4 (0.007)	0.9 (0.009)

for R95P (Fig. 7a). The largest values of R95P are observed in the upper regions of the Irrawaddy, Ganges, and Brahmaputra basins (Table 9). The lower irrigated plains in the eastern part of the Ganges basin show a coherent increasing trend in contrast to the urban western part, which shows mostly decreasing trends.

The annual spatial trends also show high variability, especially in the southern, eastern, and western parts (Fig. 7b). While the Ganges basin shows consistent and significant increases in R95P trends in the upstream regions, the Brahmaputra basin shows an increase in the western part and a significant decrease in the eastern parts. For some grid cells, the decrease in R95P is exceptionally high (30–40 mm yr⁻¹). However, the basin average annual R95P trends show a decreasing trend of 2–4 mm yr⁻¹, which is again due to the spatial aggregation. The lower reaches of the Yangtze and the Yellow show a higher degree of decreasing trends as compared with the upper and middle reaches. The Kunlun Mountains regions of the eastern Tarim show a considerable increase in R95P as compared with the decreasing trend in the western Tien Shan mountainous regions. The western basins show decreases in R95P, although the trends are not spatially coherent. The urban area of the Indus, especially around Islamabad and Lahore in Pakistan, shows a significant reduction in R95P. Interestingly, the lower irrigated regions in the Indus basin show a slight increase in R95P. Monsoon and annual R95P patterns are similar apart from western basins, where the direction of the trend is reversed (Fig. 7b).

5) CONSECUTIVE NUMBER OF DRY DAYS (CDD)

On an annual scale, the upper and lower part of the catchments shows distinct differences in CDD, in particular for the western and interior basins (Fig. 8a). The average number of CDD is highest in the upper Helmand basin, 135 days yr⁻¹,

followed by the interior basins and the lowest (~19 days yr⁻¹) in the Balkash basin (Table 10). Shi et al. (2018) reported similar values for the Tarim basin.

The spatial annual trend patterns over the region correlate with the average CDD distribution, as the areas with higher CDD have higher trends (Fig. 8b). The Helmand basin, which has the highest number of annual CDD, shows the highest positive trend of 0.55 days yr⁻¹ (Table 10). The basin average trend in western basins shows heterogeneous signals as the Helmand and Amu Darya basins show a large increasing trend (0.16–0.32 days yr⁻¹) as compared with a small (0–0.08 days yr⁻¹) decreasing trend in the Indus, Syr Darya, and Balkash basins (Fig. 8b). The decreasing trend in the TP is consistent with the increasing trends in annual precipitation, R10, RX5, and R95P. Sigdel and Ma (2017) reported a trend of 4.2 days decade⁻¹ for the southern slope of the Central Himalayan region of Nepal, which is comparable to our findings of 0.25–0.75 days yr⁻¹ (Fig. 8b). However, the authors reported a smaller but significant trend of 0.9 days decade⁻¹ for the northern slope of Central Himalayas in the TP in contrast to this study. Their estimates were based on the simple average of data from three observed stations with opposite trends, and it could be a possible reason for the differences. Our results in the middle and lower reaches of Yangtze are in line with the observed trend of -2–2 days decade⁻² reported for 1961–2015 (Shi et al. 2018).

All western, interior, and northern basins show increasing summer CDD trends except the Helmand (Fig. 8c). The spatial patterns of summer trends are significant for the eastern part of the Indus among the western basins. Interestingly, the Yangtze basin among the eastern basins shows a consistent significant increase in summer CDD for all upper parts. In the post-monsoon season, all the interior basins show a decreasing trend in contrast to the summer CDD (Fig. 8d).

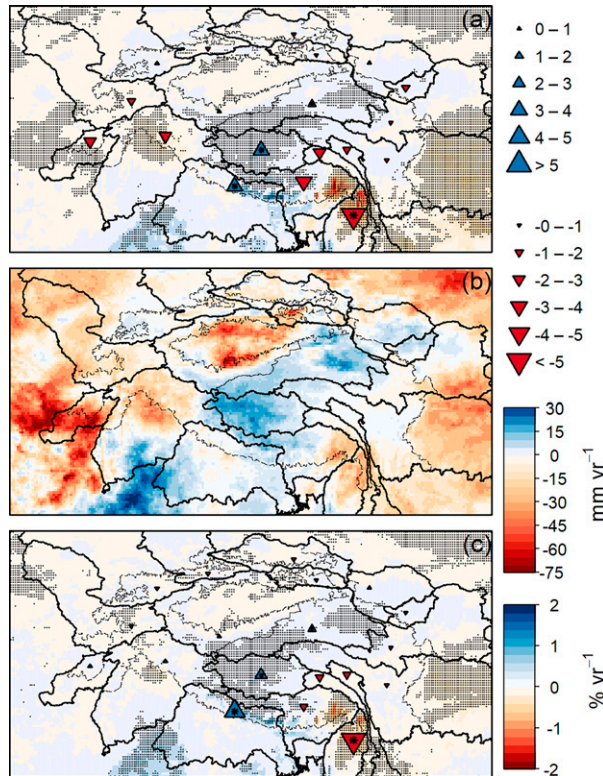


FIG. 4. Mean annual average trend for precipitation estimated using Sen's slope, expressed as (a) millimeters per year and (b) percent per year. (c) Mean annual average trend for monsoon precipitation (mm yr^{-1}) estimated using Sen's slope. Stippling represents areas with Kendall's significance at $p < 0.05$. The triangles, blue upward for an increase and red downward for a decrease, represent the upper-basin-averaged precipitation trends.

d. Trends in compounding extremes of temperature and precipitation

All the western basins show decreasing spatial trends in the number of days when the 95th quantile of precipitation (P95) is exceeded except for the Syr Darya basin (Fig. 9a). The interior basins show a significant increase in P95 except for a decrease in the TIW basin. Among the southern basins, the Ganges and Irrawaddy basins show a significant increase and decrease in P95, respectively. Again, the Brahmaputra shows mixed patterns in the spatial P95 trend in the eastern and western regions. The eastern basins show a mixed pattern in P95 trends as the upper Yangtze and Yellow show a small increase while the others show decreasing P95 trends.

In contrast to P95, the days when the 95th quantile of temperature (T95) shows a consistently increasing trend over the entire HMA. All the upper basins show significant increases in T95. Interestingly, the lower Indo-Gangetic plains show a decrease in the number of T95. Nonhomogeneous spatial patterns are observed in the TP, where the western part shows a decrease in T95 as compared with an increasing trend for the eastern part.

COMP95 shows a significant increasing trend for the interior, southern, and eastern basins. The western part of TIE

shows the highest increase ($0.2\text{--}0.25 \text{ days yr}^{-1}$) in COMP95 trends over the entire HMA, as reported by other studies (You et al. 2008; Zhao et al. 2010). Among the eastern basins, the Yangtze and Yellow basin show higher and substantial trends in COMP95. Whereas the COMP95 trends are significant in the eastern part of the Ganges, the Brahmaputra, on the other hand, shows a significant trend for the western part.

5. Discussion

a. Regional patterns in ERA5 and comparison with previous findings

1) INTERIOR BASINS

For the TP, we find a warming trend that is predominant in winter. On the basis of observed data, Yan and Liu (2014) reported a trend of $0.32^\circ\text{C decade}^{-1}$ ($\sim 1.58^\circ\text{C}$ increase for 1961–2012), lower in magnitude as compared with our estimate of $\sim 2.12^\circ\text{C}$ over 40 years (Fig. 2b; Table 4). Further, they reported the highest warming trend in winters, similar to our results. Enhanced warming trends over TP are also reported by recent regional and global studies (Duan and Xiao 2015; Pepin et al. 2015; Ren et al. 2017). However, at altitudes above 5000 m MSL, Gao et al. (2018) did not find any elevation-dependent warming trend for the past (1984–2011) and future. Warming trends calculated from ERA5 at high altitudes do not show any evidence of enhanced warming (Fig. A2 in the appendix). Chen et al. (2006), based on observed station data, reported the temperature has increased for the Tarim basin at the annual rate of $0.03^\circ\text{C yr}^{-1}$ for 1955–2000. We find similar positive increasing trends for the TIE ($\sim 0.04^\circ\text{C yr}^{-1}$) and TIW ($\sim 0.03^\circ\text{C yr}^{-1}$) (Table 4). The seasonal trends are also comparable to results that are based on observed station data (Xu et al. 2010).

The second important finding for the TP is the increase in precipitation (Figs. 10 and 11b). Precipitation changes in the region are less consistent than the temperature changes. Zhong et al. (2019), reported an increase in precipitation of 0.78 mm yr^{-1} for 1980–2014, resulting in a $\sim 27 \text{ mm}$ increase over the period. This trend is much lower than our estimate 3.57 mm yr^{-1} ($\sim 140 \text{ mm}$ increase over the 40 years). Besides, the authors reported a different trend of 1.23 mm yr^{-1} for 1999–2014, which still is lower than our estimates. A wetting trend for TP, similar to results from this study, is also widely reported (Yang et al. 2011; C. Zhang et al. 2019).

Similarly, an increasing precipitation trend (0.69 mm yr^{-1}), based on observed station data, is reported for the Tarim basin (Chen et al. 2006). We report a positive trend for TIE (1.63 mm yr^{-1}) and TIW (0.14 mm yr^{-1}). Even though absolute values differ, either due to different levels of spatial and temporal aggregation or biases in the ERA5, the direction of the trends is in line with our findings. A similar positive increase is seen for RX5, R10, and R95P for all interior basins. The interior basins, in contrast to other regions, show a decreasing trend in annual CDD. Moreover, COMP95 shows a consistent increase in the number of extremely warm and wet days over the interior basins.

TABLE 6. Average precipitation (mm) for the reference time period (1979–2018) selected for the analysis. The numbers inside the parentheses represent the trend (mm yr⁻¹), and boldface numbers represent the significance of trend at $p < 0.05$ level.

Basin	Annual	DJF	MAM	JJAS	ON
Brahmaputra	1978 (−2.245)	171 (− 0.891)	460 (−0.410)	1189 (−1.471)	158 (−0.031)
Ganges	1755 (5.018)	167 (−0.523)	252 (−0.196)	1249 (5.495)	87 (−0.087)
Irrawaddy	3593 (− 24.725)	279 (− 2.85)	768 (−3.015)	2236 (− 13.746)	310 (− 3.858)
Mekong	1035 (−1.368)	65 (− 0.334)	180 (0.242)	690 (−0.881)	99 (−0.324)
Salween	1096 (−2.306)	85 (− 0.610)	220 (−0.181)	686 (−1.421)	106 (−0.181)
Yangtze	1108 (−0.134)	66 (−0.114)	215 (0.255)	710 (−0.119)	116 (−0.239)
Yellow	740 (−0.064)	35 (−0.012)	148 (0.153)	482 (−0.307)	75 (0.105)
Amu Darya	678 (−1.288)	186 (−0.045)	265 (−0.747)	139 (−0.521)	87 (−0.025)
Lake Balkash	877 (−0.279)	88 (0.146)	236 (−0.372)	444 (−0.116)	110 (0.236)
Helmand	367 (−2.111)	174 (−1.470)	153 (−1.556)	14 (−0.038)	27 (0.483)
Indus	837 (−1.984)	198 (−0.056)	242 (− 2.13)	335 (0.439)	62 (−0.179)
Syr Darya	941 (1.101)	152 (0.670)	305 (−0.662)	356 (0.109)	127 (0.232)
Alaguy	218 (−0.468)	13 (0.042)	52 (0.113)	135 (−0.49)	19 (−0.116)
Pai-t'a Ho	633 (−1.071)	28 (−0.092)	123 (−0.234)	428 (−0.921)	55 (0.016)
Jo-Shui	395 (0.573)	19 (−0.034)	77 (0.073)	274 (0.660)	26 (0.020)
Junggar	387 (−0.183)	25 (0.054)	98 (0.014)	225 (−0.214)	39 (−0.002)
Plateau of Tibet Interior	444 (3.565)	15 (−0.072)	57 (0.281)	353 (3.196)	19 (0.002)
Tarim Interior East	305 (1.625)	17 (0.004)	63 (0.015)	209 (1.447)	17 (0.121)
Tarim Interior West	371 (0.143)	27 (0.106)	89 (−0.181)	229 (0.469)	26 (0.055)

The annual SPA over the entire interior basin shows an increasing trend, in contrast to all the other regions, which show a significant decrease in precipitation (Fig. 11b). A similar increasing trend is observed for the annual STA. The HWDI

and COMP95 occurrences also show a rising frequency in recent years. The combination of increasing precipitation with no significant changes in R10 implies mainly low to medium rainfall episodes are increasing in the region. Therefore, the TP has become warmer and wetter in recent decades, and this trend has been reported to continue in the future (Bonekamp et al. 2021; Krishnan et al. 2019; Li et al. 2010). Even though the precipitation-related spatial and seasonal trends are non-homogenous, the basin aggregated annual trends show an increase in precipitation extremes in the Tarim basin. Although the reported projected changes vary significantly, on the whole the precipitation and temperature are projected to increase in the interior basins in the future (Su et al. 2013; Zhou et al. 2014).

2) WESTERN BASINS

For this region, we find a general warming and drying trend that is not consistent across all seasons and indicators. Limited observed station data from this region has resulted in a limited number of studies in comparison with other parts of the HMA. Other studies have reported a warming trend (0.1–0.2°C decade⁻¹) and a small increasing precipitation trend in the Helmand region of Afghanistan (Krishnan et al. 2019; Outbudin et al. 2019). Similarly, Aich et al. (2017), reported an increase of 0.7°C (1980–2010) and 1.2°C (1950–80) in temperature along with a 0%–10% change in precipitation in the Helmand region. Our results show a relatively higher warming trend of ~0.05°C yr⁻¹ and a similar small wetting trend for precipitation in this region. Winter and autumn warming trends calculated from ERA5 at high altitudes show slight evidence of enhanced warming for the Amu Darya and Syr Darya basins (Fig. A1 in the appendix). The consistent warming trends for the Amu Darya, Syr Darya, and Balkash basins are in line with an observed increasing trend of 0.032°C yr⁻¹

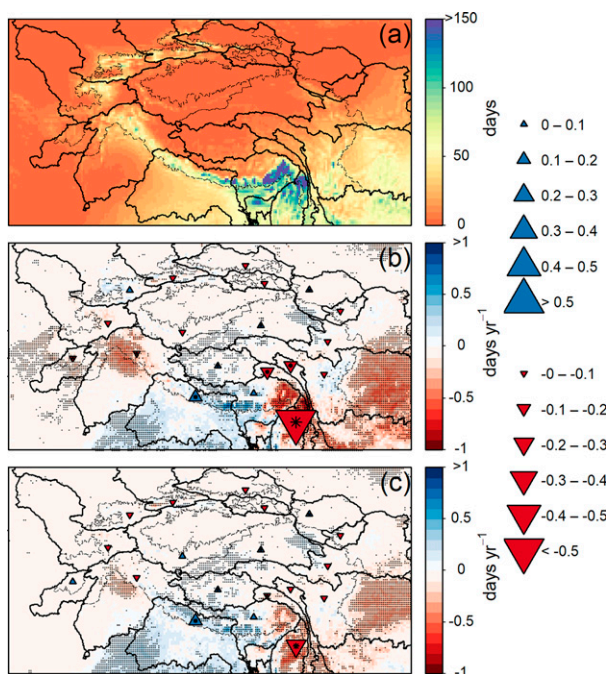


FIG. 5. (a) Mean annual average R10 (days) over HMA for 1979–2018, and the trend in R10 (days yr⁻¹) for (b) annual and (c) monsoon season estimated using Sen's slope. Stippling represents areas with Kendall's significance at $p < 0.05$. The triangles, blue upward for an increase and red downward for a decrease, represent the upper-basin-averaged R10 days trends.

TABLE 7. Average R10 (days) for the reference time period (1979–2018) selected for the analysis. The numbers inside the parentheses represent the trend (days yr^{-1}), and boldface numbers represent the significance of trend at $p < 0.05$ level.

Basin	Annual	DJF	MAM	JJAS	ON
Brahmaputra	55 (0.002)	4.5 (-0.028)	12.8 (0)	34 (0.038)	3.8 (0.001)
Ganges	51.2 (0.146)	4.6 (-0.017)	6.5 (-0.021)	38.6 (0.176)	1.6 (-0.006)
Irrawaddy	112.3 (-0.591)	9.1 (-0.113)	25.6 (-0.102)	68.9 (-0.25)	8.7 (-0.091)
Mekong	27.3 (-0.1)	0.9 (-0.005)	3.3 (0.01)	21.4 (-0.086)	1.8 (-0.011)
Salween	27.8 (-0.144)	1.3 (-0.014)	4.8 (-0.013)	19.9 (-0.097)	1.9 (-0.009)
Yangtze	29.7 (-0.01)	0.5 (-0.003)	4.6 (0.025)	22.3 (-0.029)	2.3 (-0.01)
Yellow	17.4 (-0.006)	0 (0)	2.5 (0.02)	13.8 (-0.014)	1.1 (-0.005)
Amu Darya	17 (-0.042)	4.8 (0.004)	7.8 (-0.022)	2.4 (-0.02)	2.1 (-0.004)
Balkash	22.3 (-0.015)	0.8 (0.001)	6 (-0.009)	13 (-0.006)	2.5 (0.004)
Helmand	10.1 (-0.09)	5.1 (-0.053)	4.2 (-0.064)	0.3 (0)	0.5 (0.006)
Indus	20.7 (-0.094)	5.4 (-0.009)	6.9 (-0.073)	7.1 (-0.005)	1.4 (-0.01)
Syr Darya	25.8 (0.044)	3.5 (0.026)	9.1 (-0.006)	9.5 (-0.004)	3.7 (0.007)
Alaguy	3.3 (-0.001)	0 (0)	0.6 (0.005)	2.5 (-0.008)	0.2 (-0.002)
Pai-t'a Ho	13.9 (-0.037)	0 (0)	1.6 (-0.003)	11.8 (-0.026)	0.5 (0)
Jo-Shui	7.7 (0.054)	0 (0)	0.8 (0.004)	6.8 (0.05)	0.1 (0.001)
Junggar	8.4 (-0.003)	0.1 (0.002)	1.9 (0.007)	5.9 (-0.005)	0.5 (0)
Plateau of Tibet Interior	5.5 (0.063)	0 (0)	0.2 (0.004)	5.3 (0.056)	0.1 (0)
Tarim Interior East	3.4 (0.04)	0 (0)	0.3 (0)	3 (0.038)	0 (0)
Tarim Interior West	4.9 (0)	0.1 (0.001)	1 (-0.005)	3.6 (0.01)	0.2 (0)

between 1975 and 2005 (M. Zhang et al. 2019). Likewise, for RX5, they reported an increasing trend (0.55 mm yr^{-1}), which is in line with our findings ($0.3\text{--}0.6 \text{ mm yr}^{-1}$). The warming trend of $0.30^\circ\text{C decade}^{-1}$ (for 1961–2005) reported for central Asia is comparable to the trends reported for the western and interior basins in our study (Peng et al. 2019). Even though there are discrepancies in the spatial patterns, the Indus and Balkash basins show consistent decreases for basin-aggregated indices for all precipitation-related indicators.

The annual SPA and STA show decreasing trends for both precipitation and temperature (Fig. 11a). While R10 and CDD frequencies show smaller variability, HWDI, and COMP95

show large variability in recent years. Given the above findings, it is clear that the western basins are warming for the most part. However, a general regional drying or wetting precipitation trend is harder to establish.

3) SOUTHERN BASINS

The temperature-related indices show a clear warming trend in annual and seasonal time scales. The warming trends reported here are in line with the findings based on ground observations (Dash et al. 2007; Dash and Mamgain 2011). There is a clear decreasing trend especially in the eastern

TABLE 8. Average RX5 (mm) for the reference time period (1979–2018) selected for the analysis. The numbers inside the parentheses represents the trend (mm yr^{-1}), and boldface numbers represent the significance of trend at $p < 0.05$ level.

Basin	Annual	DJF	MAM	JJAS	ON
Brahmaputra	148.6 (-0.409)	35.6 (0.012)	79.5 (0.014)	142.5 (-0.294)	53.9 (-0.138)
Ganges	182.5 (0.441)	50.8 (-0.214)	56.6 (-0.106)	178.7 (0.487)	36.2 (-0.035)
Irrawaddy	284.3 (-1.808)	72.2 (-0.045)	156.6 (-0.121)	274 (-1.595)	116.8 (-0.934)
Mekong	76 (-0.184)	17.7 (0.021)	40.2 (0.176)	72.7 (-0.147)	35.6 (-0.061)
Salween	78.8 (-0.322)	20.7 (-0.004)	45.3 (0.065)	75.2 (-0.209)	36.2 (-0.044)
Yangtze	77.7 (-0.02)	14.6 (-0.001)	41.5 (0.153)	76.8 (-0.008)	33 (-0.034)
Yellow	58.5 (0.064)	8.6 (0.01)	31.6 (0.09)	58 (0.068)	24.7 (-0.009)
Amu Darya	55.5 (0.083)	39.5 (0.053)	49 (0.059)	26.2 (-0.07)	29 (-0.047)
Balkash	61 (-0.095)	19.7 (0.045)	45.2 (-0.091)	56.9 (-0.092)	31.3 (0.142)
Helmand	60.9 (0.008)	49.5 (0.164)	45.5 (-0.645)	9.3 (-0.006)	14.4 (0.26)
Indus	87.9 (-0.047)	53.7 (0.184)	57.5 (-0.44)	67.1 (0.006)	25.5 (-0.111)
Syr Darya	66.8 (-0.026)	35.1 (0.178)	54.8 (-0.14)	49.4 (-0.056)	39.1 (0.154)
Alaguy	25.5 (-0.025)	4.6 (0.016)	13.8 (0.034)	23.8 (-0.051)	8.2 (-0.057)
Pai-t'a Ho	56.2 (0.014)	6.9 (-0.03)	25.9 (-0.016)	55.9 (0.056)	18.2 (0.05)
Jo-Shui	41.6 (0.095)	5.3 (-0.028)	18.9 (-0.011)	40.9 (0.107)	10 (-0.005)
Junggar	38 (0.016)	7.3 (0.026)	22.8 (0)	36.2 (0.019)	13.8 (-0.008)
Plateau of Tibet Interior	43.4 (0.193)	4.3 (-0.004)	13.8 (0.075)	43.4 (0.193)	7.6 (-0.013)
Tarim Interior East	30 (0.186)	4.1 (0.004)	14.7 (-0.006)	29.7 (0.184)	6.3 (0.034)
Tarim Interior West	36.2 (0.006)	7.8 (0.036)	22.1 (-0.063)	34 (0.036)	10.6 (0.019)

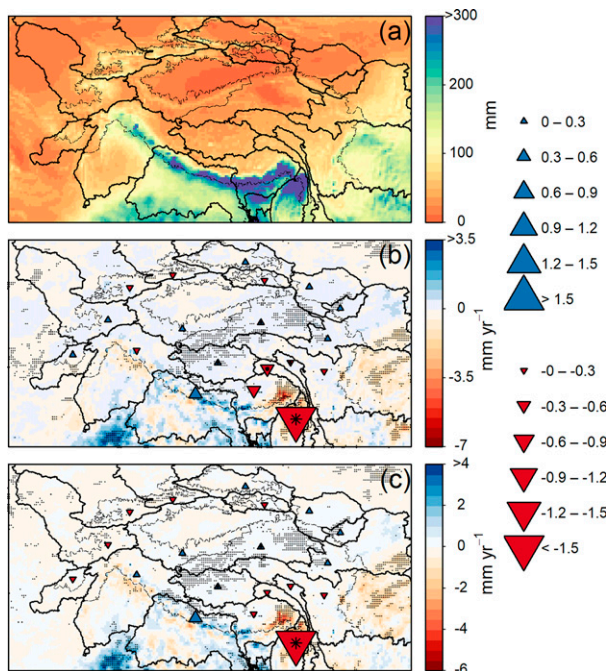


FIG. 6. As in Fig. 5, but for mean annual maximum RX5 precipitation sum (mm) and trend in RX5 (mm yr^{-1}).

Brahmaputra and Irrawaddy across all precipitation indices during the monsoon season in this region. The greenhouse gas (GHG) and anthropogenic aerosols induced warming of the Indian ocean leading to the weakening of the Indian summer monsoon explains the negative trends in annual precipitation in the southern basins (Ramanathan and Carmichael 2008; Saha et al. 2014; Saha and Ghosh 2019). Despite the variability in absolute numbers, the decreasing trends in the monsoon months for the historical climate have been reported by several studies in the Brahmaputra and the Ganges basin (Bisht et al. 2018; Choi et al. 2009; Dimri et al. 2019; Immerzeel 2008; Khandu et al. 2017; Mishra and Singh 2010; Palazzi et al. 2013). Contrastingly, Roy and Kaur (2000) reported no trend in monsoon precipitation in the upper Irrawaddy basin and did not find any direct correlation between El Niño and monsoon precipitation. Consistent with our findings, no significant trends for RX5 were reported for the historical climate in the upper Irrawaddy basin (Caesar et al. 2011; Ghimire et al. 2019).

Similar decreasing and increasing trends are observed for SPA and STA for the southern basins, respectively (Fig. 11d). Interestingly, for the past decade, the SPA and STA show higher negative and positive anomalies, which would suggest more dry and warm conditions favoring heatwave and droughts. The R10 index is highest for southern basins in comparison with other regions in HMA. While CDD remains in general similar, the HWDI and COMP95 occurrences show increasing trends in the recent past. Thus, the warming trends are evident in the region. However, drying or wetting trends are harder to establish.

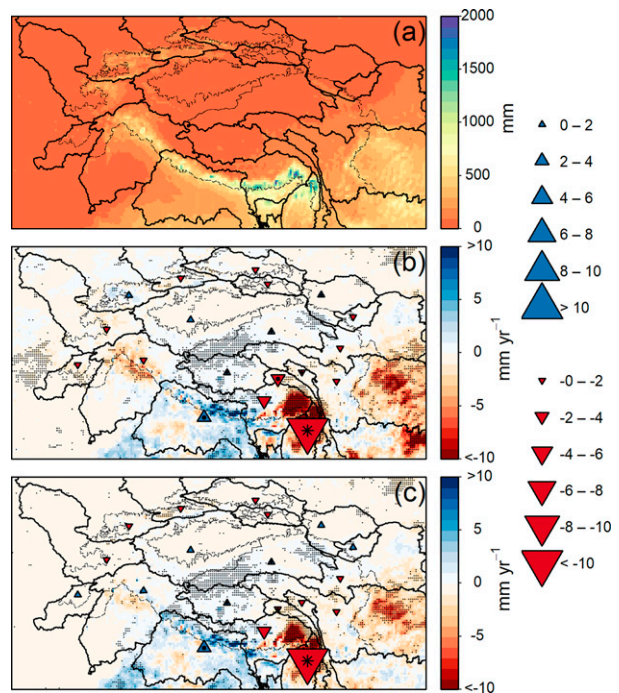


FIG. 7. As in Fig. 5, but for mean annual average R95P precipitation over TP (mm) and trend in R95P (mm yr^{-1}).

4) EASTERN BASINS

Warming trends are coherent in all the eastern basins. The warming trends ($0.03^{\circ}\text{--}0.04^{\circ}\text{C yr}^{-1}$) reported here are comparable to the observed trends (Cao et al. 2013, 2017; You et al. 2008). The temperature-related extreme indices unanimously show increasing trends in all the basins except the Yellow basin. Similarly, drying trends are also coherent in all the eastern basins. A decrease of $2\text{--}4 \text{ mm yr}^{-1}$ in the Salween and Mekong basins is comparable to the observed trends (Fan and He 2015; Li et al. 2010). The drying patterns are consistent with trends in the extreme indices in all the basins except the Yellow basin. Again, the SPA and STA show decreasing and increasing trends for precipitation and temperature, respectively. However, the former is not statistically significant (Fig. 11c). CDD frequencies are the lowest among the other regions in HMA. While variability in CDD and R10 occurrences are small, the COMP95 and HWDI occurrences show an increasing trend for the most recent years. Given the above findings, it is clear that the East Asian basins are warming and drying for most parts.

5) NORTHERN BASINS

The annual temperature trends are coherently increasing ($0.02^{\circ}\text{--}0.05^{\circ}\text{C yr}^{-1}$), in all the northern basins and are in line with observed trends ($0.2^{\circ}\text{--}0.4^{\circ}\text{C decade}^{-1}$) reported for the Junggar and Alaguy basins (Xu et al. 2018). The winter temperature trends are decreasing in these basins in contrast to other regions of HMA. These winter trends are also in contrast with the trends reported by Xu et al. (2018). They

TABLE 9. Average R95P (mm) for the time period (1979–2018) selected for the analysis. The numbers inside the parentheses represent the trend (mm yr⁻¹), and boldface numbers represent the significance of trend at $p < 0.05$ level.

Basin	Annual	DJF	MAM	JJAS	ON
Brahmaputra	415.1 (0.062)	6.8 (−0.323)	73.7 (− 2.505)	314.2 (−0.163)	20.3 (− 0.163)
Ganges	448.1 (−0.026)	32.8 (−0.152)	24.3 (3.064)	377 (0.025)	13.9 (0.025)
Irrawaddy	793.2 (−0.051)	15.8 (−0.302)	111.1 (−11.539)	606.3 (−1.012)	60 (−1.012)
Mekong	176.8 (−0.01)	5.2 (0.085)	22.8 (−0.736)	134.4 (−0.134)	14.4 (−0.134)
Salween	192.9 (−0.026)	5.8 (−0.047)	31.4 (−1.48)	139.9 (−0.118)	15.8 (−0.118)
Yangtze	200.7 (0.002)	1 (0.185)	23.8 (− 0.355)	166.8 (−0.032)	9 (− 0.032)
Yellow	131.2 (0)	0 (0.133)	13.7 (−0.269)	113.6 (0.003)	3.9 (0.003)
Lake Balkash	150.5 (0.004)	2.9 (− 0.015)	39.7 (−0.279)	94.5 (0.081)	13.4 (0.081)
Amu Darya	118.3 (−0.003)	28.3 (−0.346)	61.9 (− 0.118)	14.2 (−0.064)	13.8 (− 0.064)
Helmand	74 (−0.127)	39.4 (−0.739)	29.6 (0)	2.5 (0)	2.5 (0)
Indus	189.4 (0.274)	46.9 (− 1.209)	61.7 (0.285)	71.5 (−0.104)	9.4 (−0.104)
Syr Darya	165.8 (0.257)	17.3 (−0.197)	65.6 (−0.152)	58.2 (0.129)	24.7 (0.129)
Alaguy	35.7 (0)	0.2 (0.066)	6.3 (−0.103)	27.4 (−0.016)	1.9 (−0.016)
Pai-t'a Ho	116.8 (0)	0 (−0.019)	8 (0.048)	106.9 (0)	1.9 (0)
Jo-Shui	68.9 (0)	0 (0.061)	5.1 (0.439)	63.2 (0)	0.5 (0)
Junggar	68.8 (0.003)	0.3 (0.029)	14.1 (−0.037)	51.1 (−0.032)	3.3 (−0.032)
Plateau of Tibet Interior	65.7 (0)	0.1 (0.032)	2.1 (0.741)	62.9 (−0.001)	0.7 (−0.001)
Tarim Interior East	45.4 (0)	0 (0.008)	3.7 (0.564)	41.5 (0)	0.2 (0)
Tarim Interior West	60 (0.007)	0.7 (−0.058)	12.6 (0.143)	44.5 (−0.009)	2.2 (− 0.009)

reported a consistent increase at all the observed station locations, across all the seasons. While HWDI increases coherently for the northern basins, the annual and monsoon precipitation decreases except for Jo Shui. The annual and monsoon precipitation is also in contrast to the trends at some locations, as reported by Xu et al. (2018). They mostly report increasing precipitation trends (5–10 mm decade⁻¹) in the middle and eastern Tien Shan. Our results show similar trends, however, for smaller spatial patches (Fig. 4). We found a decreasing trend for R10 and an increasing trend for RX5

and COMP95. While SPA shows no changes, STA increases. The HWDI and COMP95 frequencies have increased in the recent past. Given the above findings, it is clear that the northern basins are warming. However, a general drying or wetting trend is again harder to establish.

In addition, the spatial patterns and trends in annual and seasonal temperature and precipitation and a range of climate change indices for large regions; HKH, entire TP (TPE), and HMA are consistent with the trends reported by previous studies (Fig. A3 in the appendix).

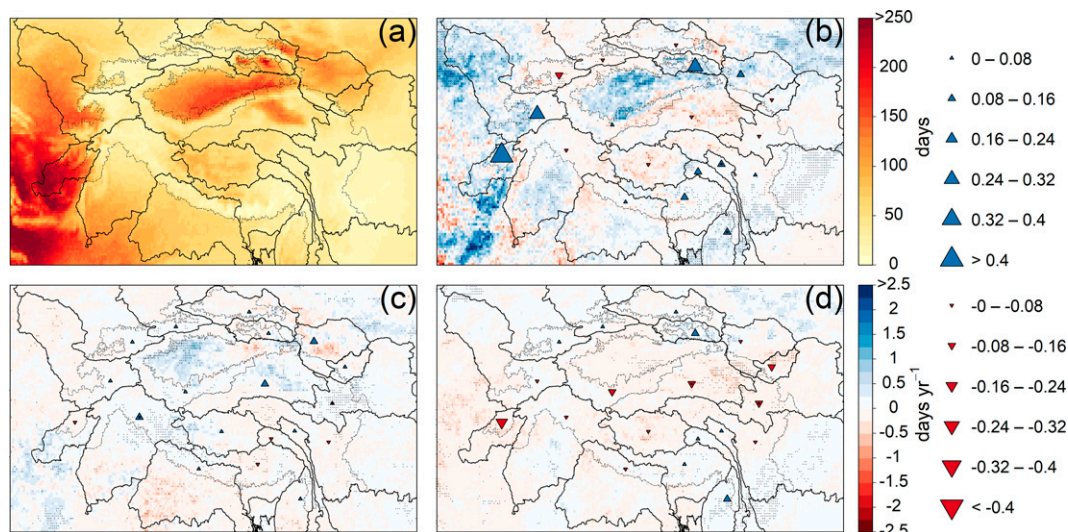


FIG. 8. (a) Mean annual average CDD (days) over entire TP for 1979–2018, and the trend in CDD (days) for (b) annual, (c) summer, and (d) post-monsoon estimated using Sen's slope. Stippling represents areas with Kendall's significance at $p < 0.05$. The triangles, blue upward for an increase and red downward for a decrease, represent the upper-basin-averaged CDD trends.

TABLE 10. Average CDD (days) for the time period (1979–2018) selected for the analysis. The numbers inside the parentheses represent the trend (days yr⁻¹), and boldface numbers represent the significance of trend at $p < 0.05$ level.

Basin	Annual	DJF	MAM	JJAS	ON
Brahmaputra	31 (0.084)	24.6 (0.014)	12.6 (−0.014)	4.8 (−0.03)	18.7 (0.034)
Ganges	33.5 (0.031)	22.7 (0.032)	14.8 (0.017)	6 (−0.027)	22.6 (−0.002)
Irrawaddy	21.9 (0.146)	19.1 (0.14)	8.7 (0.009)	1.8 (0.01)	12.8 (0.109)
Mekong	27.9 (0.105)	25 (0.11)	12.1 (0.014)	5.1 (0.011)	15.7 (0.021)
Salween	26 (0.096)	22.8 (0.089)	11.4 (−0.022)	5.2 (−0.005)	14.6 (0.028)
Yangtze	28 (0.038)	25 (0.053)	11.5 (−0.014)	4.9 (0.014)	15.1 (−0.001)
Yellow	30.3 (−0.047)	26.6 (0.027)	13 (0.077)	7.1 (0.041)	17.1 (− 0.11)
Amu Darya	48.5 (0.254)	13.8 (−0.024)	11.3 (0.01)	41.4 (0.132)	17.7 (−0.029)
Balkash	18.9 (−0.045)	16.3 (−0.025)	9.9 (0.044)	9.7 (−0.021)	11.2 (0.005)
Helmand	135.4 (0.546)	17.9 (0.208)	23.5 (−0.008)	98 (0.271)	35.3 (−0.176)
Indus	39 (−0.003)	18.4 (−0.002)	15.7 (0.083)	19.5 (− 0.077)	26.5 (−0.037)
Syr Darya	22.5 (−0.088)	15.1 (−0.069)	8.9 (0.03)	14.7 (−0.035)	12.3 (0.011)
Alaguy	66.1 (0.279)	50.3 (−0.059)	33 (0.032)	33 (0.079)	30.6 (0.158)
Pai-t'a Ho	32.1 (−0.068)	28.4 (0.065)	13.7 (0.079)	8 (0.046)	17.9 (−0.111)
Jo-Shui	48.8 (0.094)	39 (−0.004)	23.5 (0.091)	16.5 (0.036)	27.6 (−0.072)
Junggar	49.4 (−0.024)	40.5 (−0.052)	25 (0.021)	22.3 (0.007)	23.7 (0.033)
Plateau of Tibet Interior	68 (−0.049)	53.9 (0.057)	29.9 (0.042)	12.7 (−0.104)	36.2 (−0.075)
Tarim Interior East	67.2 (−0.071)	50.2 (−0.111)	28.2 (0.114)	19.5 (−0.03)	35.7 (− 0.122)
Tarim Interior West	55.9 (0.013)	39.7 (−0.15)	24.5 (0.054)	20.2 (0.071)	30.9 (−0.083)

b. Implications for extreme events and hazards

The trends in extreme indicators may have some implications to floods or droughts. During the monsoon months, especially the Indus, southern and eastern basins experience severe concurrent floods. Precipitation indices, RX5 and

R95P, over the interior and southern basins show a small increasing trend. Studies based on glacio-hydrological modeling show general seasonal shifts and an increase in the frequency and intensity of the extreme discharge in the upper Indus,

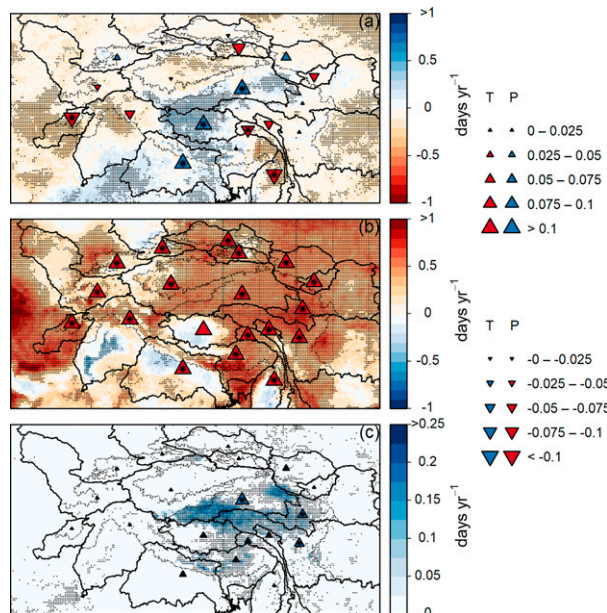


FIG. 9. Trend (days yr⁻¹) for (a) precipitation and (b) temperature greater than 95th quantile over the entire TP for 1979–2018, along with (c) trend (days yr⁻¹) when both precipitation and temperature exceed 95th quantile. Stippling represents areas with Kendall's significance at $p < 0.05$. The triangles (blue upward for precipitation P and red upward for temperature T increase, and vice versa) represent the upper-basin-averaged COMP95 trends.

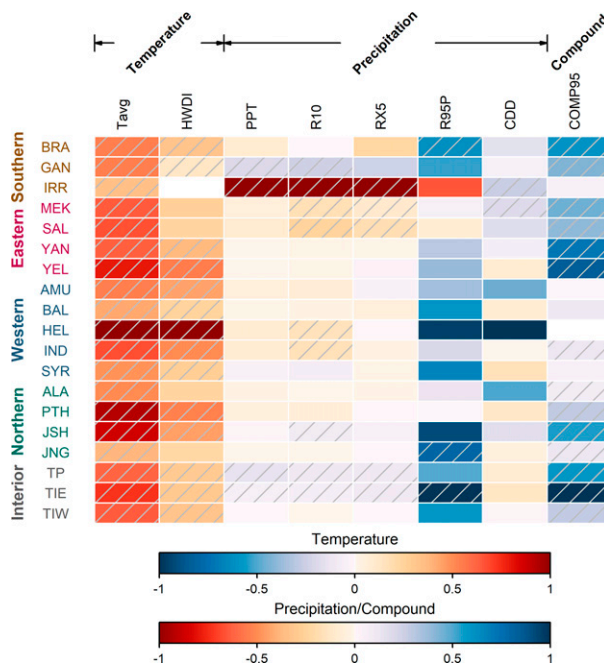


FIG. 10. Summary of upstream area-aggregated annual trends. For each indicator [average temperature (Tavg), heatwave duration index (HWDI), annual precipitation (PPT), heavy precipitation days (R10), 5-day maximum precipitation (RX5), wet days precipitation (R95P), consecutive dry days (CDD), and compound extremes (COMP95)], the trends are scaled with the absolute maximum value among the basins. The gray hatching represents the significance of the trend at $p < 0.05$.

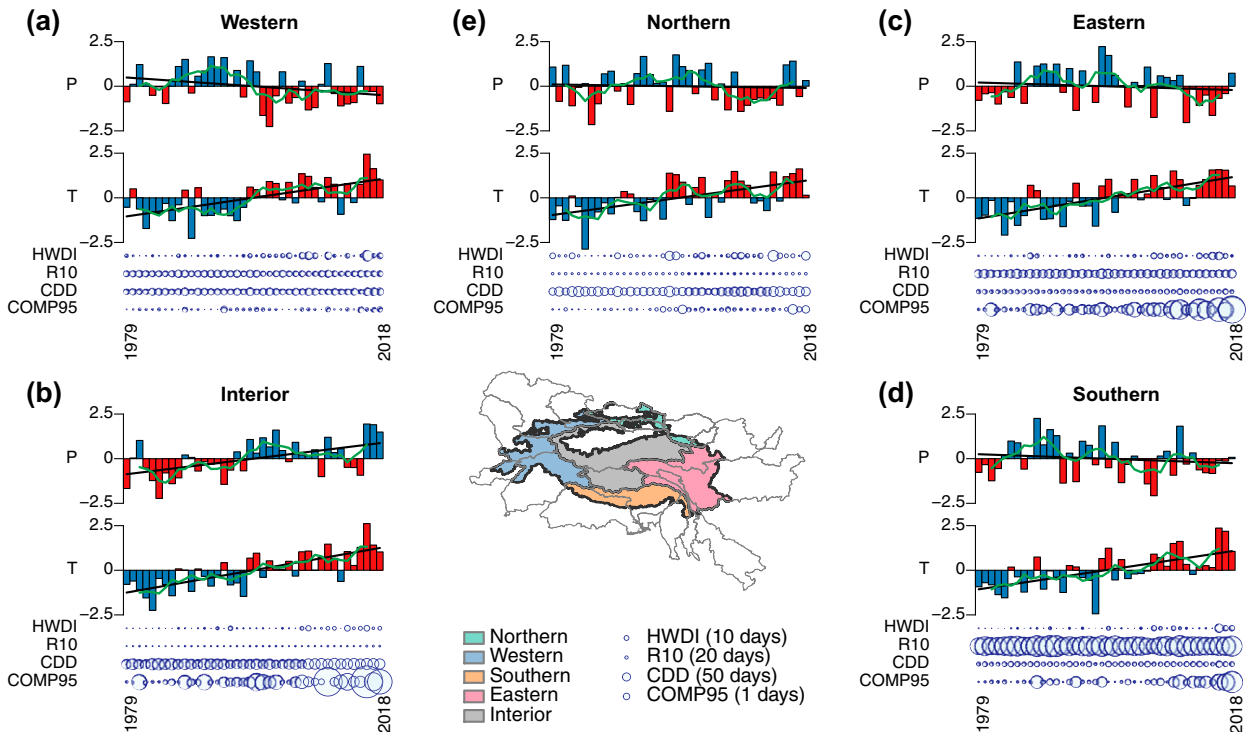


FIG. 11. (a)–(e) Area-aggregated trend in precipitation and temperature and the annual value of extreme indices for different regions, as shown in the center-bottom base map. The first two rows in (a)–(e) represent the standardized precipitation and temperature anomalies, respectively. The blue or red color represents a positive or negative anomaly, respectively, for precipitation or temperature. The x axis represents the years 1979–2018, the black line represents the linear trend, and the green line represents the moving 5-yr average. The bubbles represent the annual value of each extreme index, with different linear scaling as specified in the legend.

Ganges, and Brahmaputra basins in the future (Khanal et al. 2021; Lutz et al. 2016; Wijngaard et al. 2017). A consistent increase in temperature and related indices may have significant impacts on the cryosphere such as shrinkage of glaciers, reduction in snow cover, permafrost degradation, changes in seasonally frozen grounds, and an increase in the frequency of snow and ice avalanches (Ballesteros-Cánovas et al. 2018; Bolch et al. 2012; Kang et al. 2010). Increased temperature-related changes result in the accelerated melting of glaciers and snow, thus increasing the risk of landslide and GLOFs (Cook and Quincey 2015; Gariano and Guzzetti 2016; Huggel et al. 2012; Immerzeel et al. 2010; King et al. 2019; Kraaijenbrink et al. 2017; J. J. Liu et al. 2014; Lutz et al. 2014; Maurer et al. 2019; Song et al. 2017; Veh et al. 2020; Zhang et al. 2015). Consequently, the increased possibility of landslide events will result in cascading hazards downstream (Kargel et al. 2016; Kirschbaum et al. 2020; de Ruiter et al. 2020).

Global and regional studies have found positive linkages between CDD and drought in the past for different spatial and temporal scales (Alexander et al. 2006; Duan et al. 2017; Frich et al. 2002; Groisman and Knight 2008; Orlowsky and Seneviratne 2012). Positive STA and negative SPA in the recent decade in the western, eastern, and southern regions may suggest favorable conditions for droughts. Increases in the CDD trend over the western (Helmand and Amu Darya), eastern (Mekong and Salween), and southern (Brahmaputra

and Ganges) basins combined with increasing temperature trends may have resulted in increasing magnitude and frequency of droughts (Dai 2013). The regions with increasing temperature and less precipitation, especially, the arid western and northern basins are at higher risk than the other regions in HMA (Qin et al. 2020). The number of extreme humid heatwaves has doubled in frequency in recent decades (Raymond et al. 2020). Our results also indicate a consistent and significant increase in basin annual average HWDI for the entire HMA in recent decades. An increased possibility of heatwaves is expected in the interior and northern basins; the TP, Tarim and the Junggar, the Alagay and the Jo-Shui during the twenty-first century (Li et al. 2019).

c. Uncertainties, limitations, and outlook

This study uses reanalysis data as an alternative to limited ground-based observations to calculate trends in extreme climate indices. Spatial inferences from the limited observed station data over the HMA are challenging to establish due to the highly variable climate. In regions lacking ground-based observation, reanalysis products provide interpolated data in time and space with a dynamical consistency between different atmospheric variables and provide physically consistent model generated information (Bengtsson et al. 2004). However, its usefulness is heavily dependent on the quality and

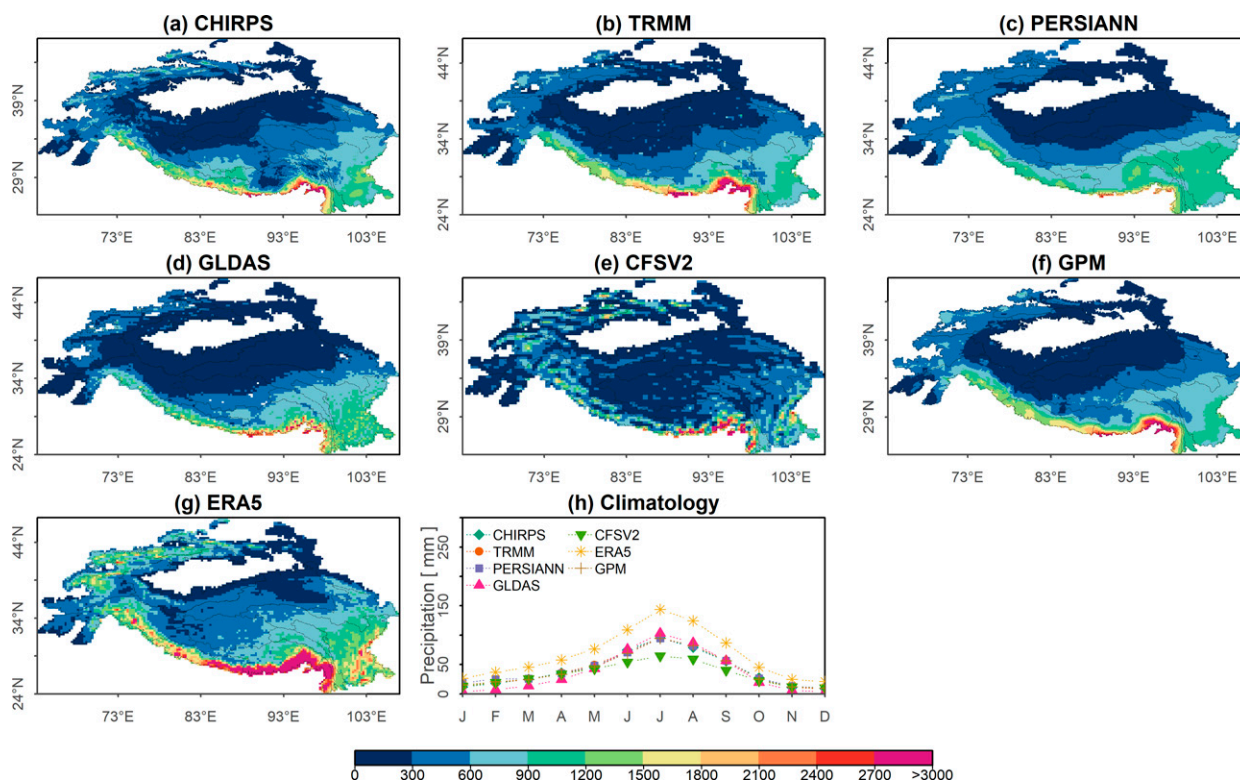


FIG. A1. Annual sum and climatology of the gridded precipitation products (gauge, satellite estimated, gauge-satellite merged, global land data assimilation system, and model simulation) for the period 2001–18.

distribution of the observation in time and space (Kalnay and Cai 2003). The presence of residual non-climatic behavior in reanalysis data poses some credibility issues on the long term trends (Thorne and Vose 2010). The ERA5 reanalysis products provide a good alternative for regions with data scarcity (Zandler et al. 2019). This study shows that the trends derived from the ERA5 are consistent with the trends based on modeled and observed data and confirm its applicability in the region. The results of this study rely heavily on the ERA5 data and potentially inherit its fundamental limitations. Even though ERA5 has shown improved performance over its predecessors for many applications, studies have found a cold bias in the ERA5 temperature, especially in midlatitudes (Cao et al. 2020; Ji and Yuan 2020; Orsolini et al. 2019; Bian et al. 2019). Most importantly, a cold bias in the order of 5°C in winter months for the eastern part of TP has been reported by several studies (Beck et al. 2020; Cao et al. 2020; Bian et al. 2019). The annual trends for threshold-related temperature indices, i.e., HWDI, will be affected by the cold biases in the ERA5 temperature. The cold biases in the winter temperature will lower the annual average temperature, thus underestimating the number of days exceeded by TXnorm plus 5°C criteria used in HWDI calculation. However, the seasonal HWDI trends except winter would remain unaffected. If the cold bias persists consistently over the entire time period, then the winter HWDI trends would also remain unchanged as it will also lower the TXnorm.

In the future, many multi-sphere observational network should be established in high altitude regions to get more

insight on meteorological and hydrological characteristics (Wang et al. 2022). Future research should consider improving the remote sensing technologies that are a reliable and cost-effective way to understand precipitation and temperature patterns and trends (Gehne et al. 2016). Moreover, long-term collaborative efforts are required to understand the climate of high-altitude regions (Locci et al. 2014; Matthews et al. 2020; Salerno et al. 2015). Additionally, improved higher resolution reanalysis products could help to a better understanding of the changes at an even smaller spatial scale, in particular for mountainous regions like HMA. For example, ERA5-Land (9 km), or the High Asia Reanalysis v2, which is based on ERA5 downscaled with WRF (Wang et al. 2020), could provide an improved understanding and more reliable estimates of the trends. The real drought indices (standardized precipitation index, Palmer drought severity index, soil moisture anomaly, Palmer hydrological drought severity index, aggregate dryness index, soil water storage, etc.), which include multiple variables like precipitation, temperature, evapotranspiration, available water content, water deficit, and solar radiation, and so on, should be used to understand the mechanism and propagation of different types of droughts (Svoboda and Fuchs 2017). Furthermore, the hydrological implications derived in this study are based solely on the meteorological drivers, i.e., precipitation and temperature. The changes in climate extremes and their co-occurrence will have a nonlinear impact on the hydrological system. Hydrological processes memorize past anomalies,

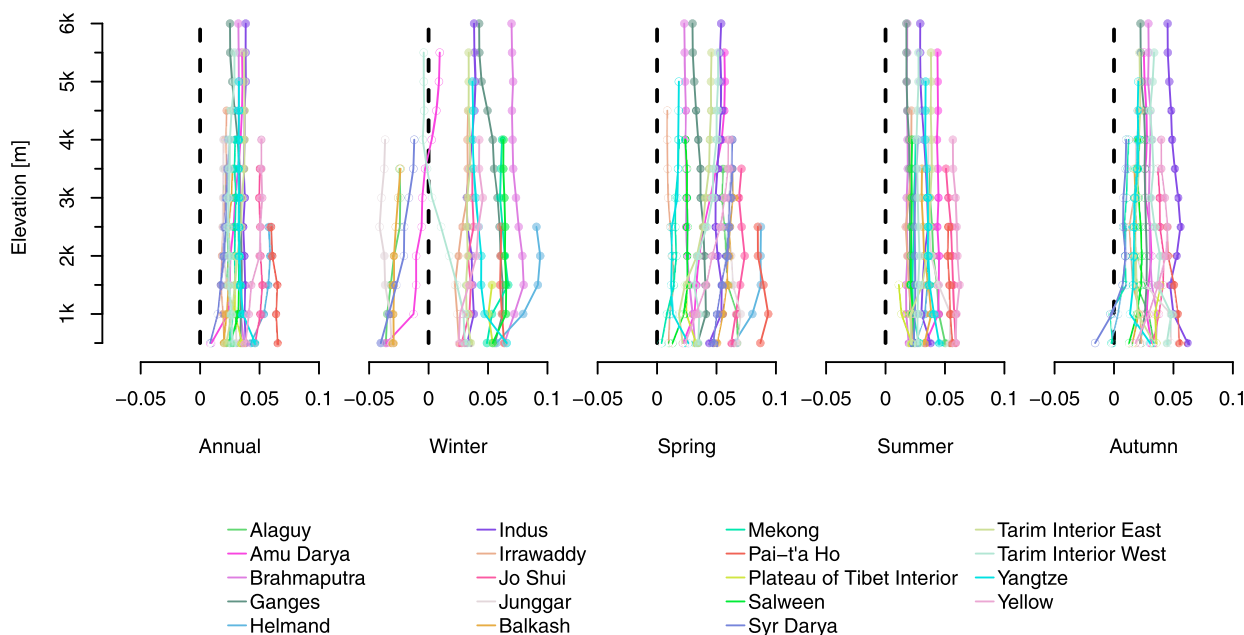


FIG. A2. The elevation-dependent mean temperature trends for the basin in HMA. The trends were calculated for 500-m bins (y axis; “k” indicates thousand). The x axis represents the trends in temperature ($^{\circ}\text{C yr}^{-1}$). The filled circles represent the statistical significance at $p < 0.05$, and vice versa.

and their effects are reflected in subsequent events or periods (Delworth and Manabe 1988; Dirmeyer et al. 2009; Khanal et al. 2019; D. Liu et al. 2014; Shinoda 2001). Therefore, a cascade of hydrological and hydraulic studies is required for more reliable and adept flood risk and drought estimation and prediction in the region.

6. Conclusions

In this study, we derive annual and seasonal historical trends in precipitation, temperature, heatwave duration index (HWDI), heavy precipitation days (R10), highest 5-day precipitation sum (RX5), wet days precipitation (R95P), consecutive dry days (CDD), the number of days when both precipitation and temperature are greater than 95th percentile of their distribution (COMP95), standardized precipitation anomaly (SPA), and standard temperature anomaly (STA) in HMA using daily ERA5 reanalysis. We conclude that ERA5 is a useful dataset to perform a region-wide, consistent historical climate analysis. We demonstrate that the trends have spatial and seasonal variability. Our results show that winter warming and summer wetting are dominant in the interior basin (Plateau of Tibet interior and Tarim). A coherent and significant increasing trend in heatwaves is observed across all regions in HMA. The results reveal that trends in heavy precipitation days show higher variability in the southern (the Ganges, the Brahmaputra, and the Irrawaddy) and eastern basins as compared with other regions in the HMA. The trends in consecutive dry days show a distinct demarcation at the boundary between lower and upper regions and are generally increasing for most basins. While the precipitation and temperature showed variable trends, their

compound occurrence shows a consistently increasing trend, in particular for the monsoon-dominated basins. The trends found in this study suggest an increase in the frequency and magnitude of extreme events and are consistent with trends reported for floods, heatwaves, and droughts in the region. Moreover, if these historical trends persist in the future, a most likely scenario, an increase in flood, drought, heatwave, landslide, and compound hazards may be expected. These hazards will have severe impacts on the overall livelihood and ecosystem of High Mountain Asia and thus require urgent adaptation policies at the local and regional level.

Acknowledgments. The project received funding from the Strategic Priority Research Program of the Chinese Academy of Sciences, Grant XDA20100300. This project was also partly funded by the European Union’s Horizon 2020 Research and Innovation Program under the Marie Skłodowska-Curie Grant 676027. We thank Jonna van Opstel for proofreading the draft paper.

Data availability statement. The ERA5 daily climate data (1979–2018) are freely available and were downloaded from the Copernicus Climate Data Store (Copernicus Climate Change Service 2017).

APPENDIX

Additional Supporting Figures

Figures A1–A3 provide additional results to support the analysis and discussion in the main text.

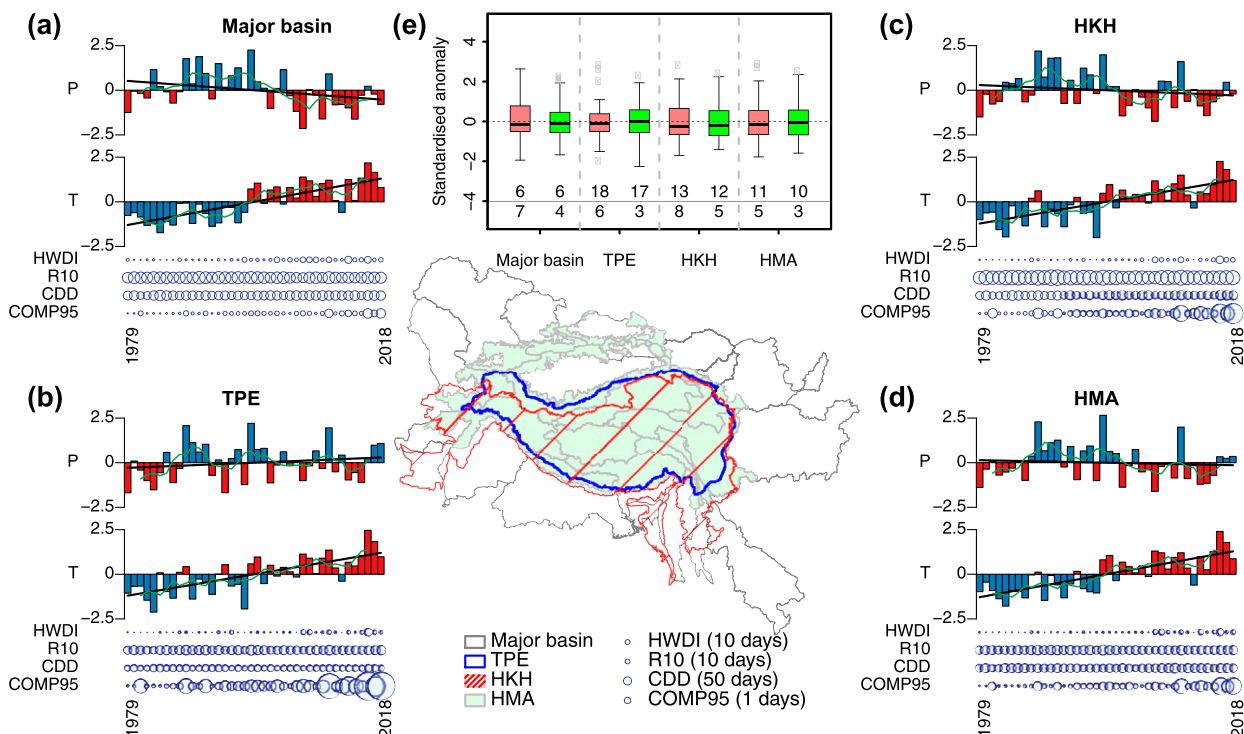


FIG. A3. (a)–(d) Area-aggregated trend in precipitation and temperature and the annual value of extreme indices for different regions, as shown in the center-bottom base map. The first two rows in (a)–(d) represent the standardized precipitation and temperature anomalies, respectively. The blue or red color represents a positive or negative anomaly, respectively, for precipitation or temperature. The x axis represents the years 1979–2018, the black line represents the linear trend, and the green line represents the moving 5-yr average. The bubbles represent the annual value of each extreme index with different linear scaling as specified in the legend. (e) The boxplots for R95P (red) and RX5 (green) standardized anomalies for 1979–2018. The numbers below the boxplots represent the percentage of pixels with positive (top row) and negative trend (bottom row) for R95P and RX5.

REFERENCES

- Aich, V., N. Akhundzadah, A. Knuerr, A. J. Khoshbeen, F. Hattermann, H. Paeth, A. Scanlon, and E. N. Paton, 2017: Climate change in Afghanistan deduced from reanalysis and coordinated regional climate downscaling experiment (CORDEX)—South Asia simulations. *Climate*, **5**, 38, <https://doi.org/10.3390/cli5020038>.
- Aizen, V. B., E. M. Aizen, J. M. Melack, and J. Dozier, 1997: Climatic and hydrologic changes in the Tien Shan, central Asia. *J. Climate*, **10**, 1393–1404, [https://doi.org/10.1175/1520-0442\(1997\)010<1393:CAHCIT>2.0.CO;2](https://doi.org/10.1175/1520-0442(1997)010<1393:CAHCIT>2.0.CO;2).
- Alexander, L. V., and Coauthors, 2006: Global observed changes in daily climate extremes of temperature and precipitation. *J. Geophys. Res.*, **111**, D05109, <https://doi.org/10.1029/2005JD006290>.
- Amato, R., H. Steptoe, E. Buonomo, and R. Jones, 2019: High-resolution history: Downscaling China's climate from the 20CRv2c reanalysis. *J. Appl. Meteor. Climatol.*, **58**, 2141–2157, <https://doi.org/10.1175/JAMC-D-19-0083.1>.
- An, W., S. Hou, Y. Hu, and S. Wu, 2017: Delayed warming hiatus over the Tibetan Plateau. *Earth Space Sci.*, **4**, 128–137, <https://doi.org/10.1002/2016EA000179>.
- Andermann, C., S. Bonnet, and R. Gloaguen, 2011: Evaluation of precipitation data sets along the Himalayan front. *Geochim. Geophys. Geosyst.*, **12**, Q07023, <https://doi.org/10.1029/2011GC003513>.
- Ashouri, H., K.-L. Hsu, S. Sorooshian, D. K. Braithwaite, K. R. Knapp, L. D. Cecil, B. R. Nelson, and O. P. Prat, 2015: PERSIANN-CDR: Daily precipitation climate data record from multisatellite observations for hydrological and climate studies. *Bull. Amer. Meteor. Soc.*, **96**, 69–83, <https://doi.org/10.1175/BAMS-D-13-00068.1>.
- Ballesteros-Cánovas, J. A., D. Trappmann, J. Madrigal-González, N. Eckert, and M. Stoffel, 2018: Climate warming enhances snow avalanche risk in the western Himalayas. *Proc. Natl. Acad. Sci. USA*, **115**, 3410–3415, <https://doi.org/10.1073/pnas.1716913115>.
- Bao, Y., and Q. You, 2019: How do westerly jet streams regulate the winter snow depth over the Tibetan Plateau? *Climate Dyn.*, **53**, 353–370, <https://doi.org/10.1007/s00382-018-4589-1>.
- Beck, H. E., A. I. J. M. van Dijk, V. Levizzani, J. Schellekens, D. G. Miralles, B. Martens, and A. de Roo, 2017: MSWEP: 3-hourly 0.25° global gridded precipitation (1979–2015) by merging gauge, satellite, and reanalysis data. *Hydrol. Earth Syst. Sci.*, **21**, 589–615, <https://doi.org/10.5194/hess-21-589-2017>.
- , E. F. Wood, T. R. McVicar, M. Zambrano-Bigiarini, C. Alvarez-Garretón, O. M. Baez-Villanueva, J. Sheffield, and D. N. Karger, 2020: Bias correction of global high-resolution precipitation climatologies using streamflow observations from 9372 catchments. *J. Climate*, **33**, 1299–1315, <https://doi.org/10.1175/JCLI-D-19-0332.1>.

- Bengtsson, L., S. Hagemann, and K. I. Hodges, 2004: Can climate trends be calculated from reanalysis data? *J. Geophys. Res.*, **109**, D11111, <https://doi.org/10.1029/2004JD004536>.
- Bhattacharya, A., and Coauthors, 2021: High Mountain Asian glacier response to climate revealed by multi-temporal satellite observations since the 1960s. *Nat. Commun.*, **12**, 4133, <https://doi.org/10.1038/s41467-021-24180-y>.
- Bian, Q., and Coauthors, 2019: Evaluation and intercomparison of multiple snow water equivalent products over the Tibetan Plateau. *J. Hydrometeorol.*, **20**, 2043–2055, <https://doi.org/10.1175/JHM-D-19-0011.1>.
- Bisht, D. S., C. Chatterjee, N. S. Raghuwanshi, and V. Sridhar, 2018: Spatio-temporal trends of rainfall across Indian River basins. *Theor. Appl. Climatol.*, **132**, 419–436, <https://doi.org/10.1007/s00704-017-2095-8>.
- Bolch, T., and Coauthors, 2012: The state and fate of Himalayan glaciers. *Science*, **336**, 310–314, <https://doi.org/10.1126/science.1215828>.
- Bonekamp, P. N. J., N. Wanders, K. van der Wiel, A. F. Lutz, and W. W. Immerzeel, 2021: Using large ensemble modelling to derive future changes in mountain specific climate indicators in a 2° and 3°C warmer world in High Mountain Asia. *Int. J. Climatol.*, **41**, E964–E979, <https://doi.org/10.1002/joc.6742>.
- Bookhagen, B., and D. W. Burbank, 2010: Toward a complete Himalayan hydrological budget: Spatiotemporal distribution of snowmelt and rainfall and their impact on river discharge. *J. Geophys. Res.*, **115**, F03019, <https://doi.org/10.1029/2009JF001426>.
- Caesar, J., and Coauthors, 2011: Changes in temperature and precipitation extremes over the Indo-Pacific region from 1971 to 2005. *Int. J. Climatol.*, **31**, 791–801, <https://doi.org/10.1002/joc.2118>.
- Cai, W., and Coauthors, 2018: Increased variability of eastern Pacific El Niño under greenhouse warming. *Nature*, **564**, 201–206, <https://doi.org/10.1038/s41586-018-0776-9>.
- Cao, B., S. Gruber, D. Zheng, and X. Li, 2020: The ERA5-land soil-temperature bias in permafrost regions. *Cryosphere*, **14**, 2581–2595, <https://doi.org/10.5194/tc-14-2581-2020>.
- Cao, L., P. Zhao, Z. Yan, P. Jones, Y. Zhu, Y. Yu, and G. Tang, 2013: Instrumental temperature series in eastern and central China back to the nineteenth century. *J. Geophys. Res. Atmos.*, **118**, 8197–8207, <https://doi.org/10.1002/jgrd.50615>.
- , Z. Yan, P. Zhao, Y. Zhu, Y. Yu, G. Tang, and P. Jones, 2017: Climatic warming in China during 1901–2015 based on an extended dataset of instrumental temperature records. *Environ. Res. Lett.*, **12**, 064005, <https://doi.org/10.1088/1748-9326/aa68e8>.
- Cheema, M. J. M., and W. G. M. Bastiaanssen, 2012: Local calibration of remotely sensed rainfall from the TRMM satellite for different periods and spatial scales in the Indus Basin. *Int. J. Remote Sens.*, **33**, 2603–2627, <https://doi.org/10.1080/01431161.2011.617397>.
- Chen, F., W. Huang, L. Jin, J. Chen, and J. Wang, 2011: Spatio-temporal precipitation variations in the arid Central Asia in the context of global warming. *Sci. China Earth Sci.*, **54**, 1812–1821, <https://doi.org/10.1007/s11430-011-4333-8>.
- Chen, Y., K. Takeuchi, C. Xu, Y. Chen, and Z. Xu, 2006: Regional climate change and its effects on river runoff in the Tarim Basin, China. *Hydrol. Processes*, **20**, 2207–2216, <https://doi.org/10.1002/hyp.6200>.
- Choi, G., and Coauthors, 2009: Changes in means and extreme events of temperature and precipitation in the Asia-Pacific network region, 1955–2007. *Int. J. Climatol.*, **29**, 1906–1925, <https://doi.org/10.1002/joc.1979>.
- Cohen, J., J. C. Furtado, M. A. Barlow, V. A. Alexeev, and J. E. Cherry, 2012: Arctic warming, increasing snow cover and widespread boreal winter cooling. *Environ. Res. Lett.*, **7**, 014007, <https://doi.org/10.1088/1748-9326/7/1/014007>.
- , and Coauthors, 2014: Recent Arctic amplification and extreme mid-latitude weather. *Nat. Geosci.*, **7**, 627–637, <https://doi.org/10.1038/ngeo2234>.
- , and Coauthors, 2020: Divergent consensus on Arctic amplification influence on midlatitude severe winter weather. *EGU General Assembly 2020, Arctic Climate Change: Governing Mechanisms and Global Implications*, EGU2020-2748, online, <https://doi.org/10.5194/egusphere-egu2020-2748>.
- Cook, S. J., and D. J. Quincey, 2015: Estimating the volume of Alpine glacial lakes. *Earth Surf. Dyn.*, **3**, 559–575, <https://doi.org/10.5194/esurf-3-559-2015>.
- Copernicus Climate Change Service, 2017: ERA5: Fifth generation of ECMWF atmospheric reanalyses of the global climate. Copernicus Climate Change Service Climate Data Store (CDS), accessed 20 May 2019, <https://cds.climate.copernicus.eu/cdsapp#!/home>.
- Cuo, L., Y. Zhang, Q. Wang, L. Zhang, B. Zhou, Z. Hao, and F. Su, 2013: Climate change on the northern Tibetan Plateau during 1957–2009: Spatial patterns and possible mechanisms. *J. Climate*, **26**, 85–109, <https://doi.org/10.1175/JCLI-D-11-00738.1>.
- Dahri, Z. H., F. Ludwig, E. Moors, S. Ahmad, B. Ahmad, S. Ahmad, M. Riaz, and P. Kabat, 2021a: Climate change and hydrological regime of the high-altitude Indus basin under extreme climate scenarios. *Sci. Total Environ.*, **768**, 144467, <https://doi.org/10.1016/j.scitotenv.2020.144467>.
- , and Coauthors, 2021b: Spatio-temporal evaluation of gridded precipitation products for the high-altitude Indus basin. *Int. J. Climatol.*, **41**, 4283–4306, <https://doi.org/10.1002/joc.7073>.
- Dai, A., 2013: Increasing drought under global warming in observations and models. *Nat. Climate Change*, **3**, 52–58, <https://doi.org/10.1038/nclimate1633>.
- Dash, S. K., and A. Mangain, 2011: Changes in the frequency of different categories of temperature extremes in India. *J. Appl. Meteor. Climatol.*, **50**, 1842–1858, <https://doi.org/10.1175/2011JAMC2687.1>.
- , R. K. Jenamani, S. R. Kalsi, and S. K. Panda, 2007: Some evidence of climate change in twentieth-century India. *Climatic Change*, **85**, 299–321, <https://doi.org/10.1007/s10584-007-9305-9>.
- Dee, D. P., and Coauthors, 2011: The ERA-Interim reanalysis: Configuration and performance of the data assimilation system. *Quart. J. Roy. Meteor. Soc.*, **137**, 553–597, <https://doi.org/10.1002/qj.828>.
- Delworth, T. L., and S. Manabe, 1988: The influence of potential evaporation on the variabilities of simulated soil wetness and climate. *J. Climate*, **1**, 523–547, [https://doi.org/10.1175/1520-0442\(1988\)001<0523:TIOPEO>2.0.CO;2](https://doi.org/10.1175/1520-0442(1988)001<0523:TIOPEO>2.0.CO;2).
- Deng, H., and Y. Chen, 2017: Influences of recent climate change and human activities on water storage variations in Central Asia. *J. Hydrol.*, **544**, 46–57, <https://doi.org/10.1016/j.jhydrol.2016.11.006>.
- de Ruiter, M. C., A. Couasnon, M. J. C. van den Homberg, J. E. Daniell, J. C. Gill, and P. J. Ward, 2020: Why we can no longer ignore consecutive disasters. *Earth's Future*, **8**, e2019EF001425, <https://doi.org/10.1029/2019EF001425>.

- Dimri, A. P., B. Bookhagen, M. Stoffel, and T. Yasunari, 2019: *Himalayan Weather and Climate and Their Impact on the Environment*. Springer, 577 pp.
- Dirmeyer, P. A., C. A. Schlosser, and K. L. Brubaker, 2009: Precipitation, recycling, and land memory: An integrated analysis. *J. Hydrometeorol.*, **10**, 278–288, <https://doi.org/10.1175/2008JHM1016.1>.
- Donat, M. G., J. Sillmann, S. Wild, L. V. Alexander, T. Lippmann, and F. W. Zwiers, 2014: Consistency of temperature and precipitation extremes across various global gridded in situ and reanalysis datasets. *J. Climate*, **27**, 5019–5035, <https://doi.org/10.1175/JCLI-D-13-00405.1>.
- Duan, A., and Z. Xiao, 2015: Does the climate warming hiatus exist over the Tibetan Plateau? *Sci. Rep.*, **5**, 13711, <https://doi.org/10.1038/srep13711>.
- Duan, Y., Z. Ma, and Q. Yang, 2017: Characteristics of consecutive dry days variations in China. *Theor. Appl. Climatol.*, **130**, 701–709, <https://doi.org/10.1007/s00704-016-1984-6>.
- Fan, H., and D. He, 2015: Temperature and precipitation variability and its effects on streamflow in the upstream regions of the Lancang-Mekong and Nu-Salween Rivers. *J. Hydrometeorol.*, **16**, 2248–2263, <https://doi.org/10.1175/JHM-D-14-0238.1>.
- Fowler, H. J., and D. R. Archer, 2006: Conflicting signals of climatic change in the upper Indus Basin. *J. Climate*, **19**, 4276–4293, <https://doi.org/10.1175/JCLI3860.1>.
- Frauenfeld, O. W., T. Zhang, and M. C. Serreze, 2005: Climate change and variability using European Centre for Medium-Range Weather Forecasts reanalysis (ERA-40) temperatures on the Tibetan Plateau. *J. Geophys. Res.*, **110**, D02101, <https://doi.org/10.1029/2004JD005230>.
- Frich, P., L. V. Alexander, P. Della-Marta, B. Gleason, M. Haylock, A. M. G. Klein Tank, and T. Peterson, 2002: Observed coherent changes in climatic extremes during the second half of the twentieth century. *Climate Res.*, **19**, 193–212, <https://doi.org/10.3354/cr019193>.
- Funk, C., and Coauthors, 2015: The climate hazards infrared precipitation with stations—A new environmental record for monitoring extremes. *Sci. Data*, **2**, 150066, <https://doi.org/10.1038/sdata.2015.66>.
- Gao, Y., F. Chen, D. P. Lettenmaier, J. Xu, L. Xiao, and X. Li, 2018: Does elevation-dependent warming hold true above 5000 m elevation? Lessons from the Tibetan Plateau. *npj Climate Atmos. Sci.*, **1**, 19, <https://doi.org/10.1038/s41612-018-0030-z>.
- Gariano, S. L., and F. Guzzetti, 2016: Landslides in a changing climate. *Earth-Sci. Rev.*, **162**, 227–252, <https://doi.org/10.1016/j.earscirev.2016.08.011>.
- Gebregiorgis, A. S., and F. Hossain, 2015: How well can we estimate error variance of satellite precipitation data around the world? *Atmos. Res.*, **154**, 39–59, <https://doi.org/10.1016/j.atmosres.2014.11.005>.
- Gehne, M., T. M. Hamill, G. N. Kiladis, and K. E. Trenberth, 2016: Comparison of global precipitation estimates across a range of temporal and spatial scales. *J. Climate*, **29**, 7773–7795, <https://doi.org/10.1175/JCLI-D-15-0618.1>.
- Ghimire, U., M. S. Babel, S. Shrestha, and G. Srinivasan, 2019: A multi-temporal analysis of streamflow using multiple CMIP5 GCMs in the upper Ayerawaddy Basin, Myanmar. *Climatic Change*, **155**, 59–79, <https://doi.org/10.1007/s10584-019-02444-3>.
- Gilbert, R. O., 1987: *Statistical Methods for Environmental Pollution Monitoring*. John Wiley and Sons, 336 pp.
- Groisman, P. Ya., and R. W. Knight, 2008: Prolonged dry episodes over the conterminous United States: New tendencies emerging during the last 40 years. *J. Climate*, **21**, 1850–1862, <https://doi.org/10.1175/2007JCLI2103.1>.
- Gu, H., Z. Yu, C. Yang, and Q. Ju, 2018: Projected changes in hydrological extremes in the Yangtze River basin with an ensemble of regional climate simulations. *Water*, **10**, 1279, <https://doi.org/10.3390/w10091279>.
- Guo, D., and H. Wang, 2012: The significant climate warming in the northern Tibetan Plateau and its possible causes. *Int. J. Climatol.*, **32**, 1775–1781, <https://doi.org/10.1002/joc.2388>.
- Guo, H., S. Chen, A. Bao, J. Hu, A. S. Gebregiorgis, X. Xue, and X. Zhang, 2015: Inter-comparison of high-resolution satellite precipitation products over Central Asia. *Remote Sens.*, **7**, 7181–7211, <https://doi.org/10.3390/rs70607181>.
- Hersbach, H., and Coauthors, 2020: The ERA5 global reanalysis. *Quart. J. Roy. Meteor. Soc.*, **146**, 1999–2049, <https://doi.org/10.1002/qj.3803>.
- Hu, X., and W. Yuan, 2021: Evaluation of ERA5 precipitation over the eastern periphery of the Tibetan Plateau from the perspective of regional rainfall events. *Int. J. Climatol.*, **41**, 2625–2637, <https://doi.org/10.1002/joc.6980>.
- Hu, Z., C. Zhang, Q. Hu, and H. Tian, 2014: Temperature changes in central Asia from 1979 to 2011 based on multiple datasets. *J. Climate*, **27**, 1143–1167, <https://doi.org/10.1175/JCLI-D-13-00064.1>.
- Huffman, G. J., and Coauthors, 2007: The TRMM Multisatellite Precipitation Analysis (TMPA): Quasi-global, multiyear, combined-sensor precipitation estimates at fine scales. *J. Hydrometeorol.*, **8**, 38–55, <https://doi.org/10.1175/JHM560.1>.
- Huggel, C., J. J. Clague, and O. Korup, 2012: Is climate change responsible for changing landslide activity in high mountains? *Earth Surf. Processes Landforms*, **37**, 77–91, <https://doi.org/10.1002/esp.2223>.
- Im, E.-S., J. S. Pal, and E. A. B. Eltahir, 2017: Deadly heat waves projected in the densely populated agricultural regions of South Asia. *Sci. Adv.*, **3**, e1603322, <https://doi.org/10.1126/sciadv.1603322>.
- Immerzeel, W. W., 2008: Historical trends and future predictions of climate variability in the Brahmaputra basin. *Int. J. Climatol.*, **28**, 243–254, <https://doi.org/10.1002/joc.1528>.
- , and M. F. P. Bierkens, 2012: Asia's water balance. *Nat. Geosci.*, **5**, 841–842, <https://doi.org/10.1038/ngeo1643>.
- , L. P. H. Van Beek, and M. F. P. Bierken, 2010: Climate change will affect the Asian water towers. *Science*, **328**, 1382–1385, <https://doi.org/10.1126/science.1183188>.
- , N. Wanders, A. F. Lutz, J. M. Shea, and M. F. P. Bierkens, 2015: Reconciling high-altitude precipitation in the upper Indus basin with glacier mass balances and runoff. *Hydrol. Earth Syst. Sci.*, **19**, 4673–4687, <https://doi.org/10.5194/hess-19-4673-2015>.
- Ji, P., and X. Yuan, 2020: Underestimation of the warming trend over the Tibetan Plateau during 1998–2013 by global land data assimilation systems and atmospheric reanalyses. *J. Meteor. Res.*, **34**, 88–100, <https://doi.org/10.1007/s13351-020-9100-3>.
- Jiang, Q., and Coauthors, 2020: Evaluation of the ERA5 reanalysis precipitation dataset over Chinese Mainland. *J. Hydrol.*, **595**, 125660, <https://doi.org/10.1016/j.jhydrol.2021.125958>.
- Jin, X.-Y., H.-J. Jin, G. Iwahana, S. S. Marchenko, D.-L. Luo, X.-Y. Li, and S.-H. Liang, 2020: Impacts of climate-induced permafrost degradation on vegetation: A review. *Adv. Climate Change Res.*, **12**, 29–47, <https://doi.org/10.1016/j.accre.2020.07.002>.
- Joyce, R. J., J. E. Janowiak, P. A. Arkin, and P. Xie, 2004: CMORPH: A method that produces global precipitation

- estimates from passive microwave and infrared data at high spatial and temporal resolution. *J. Hydrometeor.*, **5**, 487–503, [https://doi.org/10.1175/1525-7541\(2004\)005<0487:CAMTPG>2.0.CO;2](https://doi.org/10.1175/1525-7541(2004)005<0487:CAMTPG>2.0.CO;2).
- Kääb, A., E. Berthier, C. Nuth, J. Gardelle, and Y. Arnaud, 2012: Contrasting patterns of early twenty-first-century glacier mass change in the Himalayas. *Nature*, **488**, 495–498, <https://doi.org/10.1038/nature11324>.
- Kalnay, E., and M. Cai, 2003: Impact of urbanization and land-use change on climate. *Nature*, **423**, 528–531, <https://doi.org/10.1038/nature01675>.
- Kang, S., Y. Xu, Q. You, W.-A. Flügel, N. Pepin, and T. Yao, 2010: Review of climate and cryospheric change in the Tibetan Plateau. *Environ. Res. Lett.*, **5**, 015101, <https://doi.org/10.1088/1748-9326/5/1/015101>.
- Kargel, J. S., and Coauthors, 2016: Geomorphic and geologic controls of geohazards induced by Nepal's 2015 Gorkha earthquake. *Science*, **351**, aac8353, <https://doi.org/10.1126/science.aac8353>.
- Khanal, S., A. F. Lutz, W. W. Immerzeel, H. de Vries, N. Wanders, and B. van den Hurk, 2019: The impact of meteorological and hydrological memory on compound peak flows in the Rhine river basin. *Atmosphere*, **10**, 171, <https://doi.org/10.3390/atmos10040171>.
- , —, P. D. A. Kraaijenbrink, B. van den Hurk, T. Yao, and W. W. Immerzeel, 2021: Variable 21st century climate change response for rivers in High Mountain Asia at seasonal to decadal time scales. *Water Resour. Res.*, **57**, e2020WR029266, <https://doi.org/10.1029/2020WR029266>.
- Khandu, A., J. L. Awange, M. Kuhn, R. Anyah, and E. Forootan, 2017: Changes and variability of precipitation and temperature in the Ganges–Brahmaputra–Meghna River Basin based on global high-resolution reanalyses. *Int. J. Climatol.*, **37**, 2141–2159, <https://doi.org/10.1002/joc.4842>.
- Khattak, M. S., M. S. Babel, and M. Sharif, 2011: Hydro-meteorological trends in the upper Indus River basin in Pakistan. *Climate Res.*, **46**, 103–119, <https://doi.org/10.3354/cr00957>.
- King, O., A. Bhattacharya, R. Bhambri, and T. Bolch, 2019: Glacial lakes exacerbate Himalayan glacier mass loss. *Sci. Rep.*, **9**, 18145, <https://doi.org/10.1038/s41598-019-53733-x>.
- Kirschbaum, D., S. B. Kapnick, T. Stanley, and S. Pascale, 2020: Changes in extreme precipitation and landslides over High Mountain Asia. *Geophys. Res. Lett.*, **47**, e2019GL085347, <https://doi.org/10.1029/2019GL085347>.
- Kosaka, Y., and S.-P. Xie, 2013: Recent global-warming hiatus tied to equatorial Pacific surface cooling. *Nature*, **501**, 403–407, <https://doi.org/10.1038/nature12534>.
- Kraaijenbrink, P. D. A., M. F. P. Bierkens, A. F. Lutz, and W. W. Immerzeel, 2017: Impact of a global temperature rise of 1.5 degrees Celsius on Asia's glaciers. *Nature*, **549**, 257–260, <https://doi.org/10.1038/nature23878>.
- , E. E. Stigter, T. Yao, and W. W. Immerzeel, 2021: Climate change decisive for Asia's snow meltwater supply. *Nat. Climate Change*, **11**, 591–597, <https://doi.org/10.1038/s41558-021-01074-x>.
- Krishnan, R., and Coauthors, 2019: Unravelling climate change in the Hindu Kush Himalaya: Rapid warming in the mountains and increasing extremes. *The Hindu Kush Himalaya Assessment*, P. Wester et al., Eds., Springer, 57–97.
- Lai, H.-W., H. W. Chen, J. Kukulies, T. Ou, and D. Chen, 2021: Regionalization of seasonal precipitation over the Tibetan Plateau and associated large-scale atmospheric systems. *J. Climate*, **34**, 2635–2651, <https://doi.org/10.1175/JCLI-D-20-0521.1>.
- Lehner, B., K. Verdin, and A. Jarvis, 2008: New global hydrography derived from spaceborne elevation data. *Eos, Trans. Amer. Geophys. Union*, **89**, 93–94, <https://doi.org/10.1029/2008EO100001>.
- Lei, X., and Coauthors, 2022: How well does the ERA5 reanalysis capture the extreme climate events over China? Part I: Extreme precipitation. *Front. Environ. Sci.*, **10**, 921658, <https://doi.org/10.3389/fenvs.2022.921658>.
- Lei, Y., J. Pan, C. Xiong, L. Jiang, and J. Shi, 2023: Snow depth and snow cover over the Tibetan Plateau observed from space in against ERA5: Matters of scale. *Climate Dyn.*, <https://doi.org/10.1007/s00382-022-06376-0>, in press.
- Li, L., S. Yang, Z. Wang, X. Zhu, and H. Tang, 2010: Evidence of warming and wetting climate over the Qinghai-Tibet plateau. *Arct. Antarct. Alp. Res.*, **42**, 449–457, <https://doi.org/10.1657/1938-4246-42.4.449>.
- Li, Y., X. Qin, Y. Liu, Z. Jin, J. Liu, L. Wang, and J. Chen, 2022: Evaluation of long-term and high-resolution gridded precipitation and temperature products in the Qilian Mountains, Qinghai-Tibet Plateau. *Front. Environ. Sci.*, **10**, 906821, <https://doi.org/10.3389/fenvs.2022.906821>.
- Li, Z., X. Guo, Y. Yang, Y. Hong, Z. Wang, and L. You, 2019: Heatwave trends and the population exposure over China in the 21st century as well as under 1.5°C and 2.0°C global warmer future scenarios. *Sustainability*, **11**, 3318, <https://doi.org/10.3390/su11123318>.
- Liu, D., G. Wang, R. Mei, Z. Yu, and M. Yu, 2014: Impact of initial soil moisture anomalies on climate mean and extremes over Asia. *J. Geophys. Res. Atmos.*, **119**, 529–545, <https://doi.org/10.1002/2013JD020890>.
- Liu, J. J., Z. L. Cheng, and P. C. Su, 2014: The relationship between air temperature fluctuation and glacial lake outburst floods in Tibet, China. *Quat. Int.*, **321**, 78–87, <https://doi.org/10.1016/j.quaint.2013.11.023>.
- Liu, X., and B. Chen, 2000: Climatic warming in the Tibetan Plateau during recent decades. *Int. J. Climatol.*, **20**, 1729–1742, [https://doi.org/10.1002/1097-0088\(20001130\)20:14<1729::AID-JOC556>3.0.CO;2-Y](https://doi.org/10.1002/1097-0088(20001130)20:14<1729::AID-JOC556>3.0.CO;2-Y).
- , Z. Cheng, L. Yan, and Z.-Y. Yin, 2009: Elevation dependency of recent and future minimum surface air temperature trends in the Tibetan Plateau and its surroundings. *Global Planet. Change*, **68**, 164–174, <https://doi.org/10.1016/j.gloplacha.2009.03.017>.
- Locci, F., M. T. Melis, F. Dessì, P. Stocchi, M. O. Akinde, V. Bønes, P. Bonasoni, and E. Vuillermoz, 2014: Implementation of a web GIS service platform for high mountain climate research: The SHARE GeoNetwork project. *Geosci. Data J.*, **1**, 140–157, <https://doi.org/10.1002/gdj3.14>.
- Lutz, A. F., W. W. Immerzeel, A. B. Shrestha, and M. F. P. Bierkens, 2014: Consistent increase in high Asia's runoff due to increasing glacier melt and precipitation. *Nat. Climate Change*, **4**, 587–592, <https://doi.org/10.1038/nclimate2237>.
- , —, P. D. A. Kraaijenbrink, A. B. Shrestha, and M. F. P. Bierkens, 2016: Climate change impacts on the upper Indus hydrology: Sources, shifts and extremes. *PLOS ONE*, **11**, e0165630, <https://doi.org/10.1371/journal.pone.0165630>.
- Madhura, R. K., R. Krishnan, J. V. Revadekar, M. Mujumdar, and B. N. Goswami, 2015: Changes in western disturbances over the Western Himalayas in a warming environment. *Climate Dyn.*, **44**, 1157–1168, <https://doi.org/10.1007/s00382-014-2166-9>.

- Mann, H. B., 1945: Nonparametric tests against trend. *Econometrica*, **13**, 245–259, [https://doi.org/0012-9682\(194507\)13:3<245:NTAT>2.0.CO;2-U](https://doi.org/0012-9682(194507)13:3<245:NTAT>2.0.CO;2-U).
- Matthews, T., and Coauthors, 2020: Going to extremes: Installing the world's highest weather stations on Mount Everest. *Bull. Amer. Meteor. Soc.*, **101**, E1870–E1890, <https://doi.org/10.1175/BAMS-D-19-0198.1>.
- Maurer, J. M., J. M. Schaefer, S. Rupper, and A. Corley, 2019: Acceleration of ice loss across the Himalayas over the past 40 years. *Sci. Adv.*, **5**, eaav7266, <https://doi.org/10.1126/sciadv.aav7266>.
- Maussion, F., D. Scherer, T. Mölg, E. Collier, J. Curio, and R. Finkelnburg, 2014: Precipitation seasonality and variability over the Tibetan Plateau as resolved by the high Asia reanalysis. *J. Climate*, **27**, 1910–1927, <https://doi.org/10.1175/JCLI-D-13-00282.1>.
- Mei, Y., E. N. Anagnostou, E. I. Nikolopoulos, and M. Borga, 2014: Error analysis of satellite precipitation products in mountainous basins. *J. Hydrometeorol.*, **15**, 1778–1793, <https://doi.org/10.1175/JHM-D-13-0194.1>.
- Merz, B., and Coauthors, 2014: Floods and climate: Emerging perspectives for flood risk assessment and management. *Nat. Hazards Earth Syst. Sci.*, **14**, 1921–1942, <https://doi.org/10.5194/nhess-14-1921-2014>.
- Mishra, A. K., and V. P. Singh, 2010: A review of drought concepts. *J. Hydrol.*, **391**, 202–216, <https://doi.org/10.1016/j.jhydrol.2010.07.012>.
- Nied, M., T. Pardowitz, K. Nissen, U. Ulbrich, Y. Hundechea, and B. Merz, 2014: On the relationship between hydro-meteorological patterns and flood types. *J. Hydrol.*, **519**, 3249–3262, <https://doi.org/10.1016/j.jhydrol.2014.09.089>.
- NOAA, 2020: Climate at a glance global time series. National Centers for Environmental Information, accessed 7 October 2020, <https://www.ncdc.noaa.gov/cag/global/time-series>.
- Orlowsky, B., and S. I. Seneviratne, 2012: Global changes in extreme events: Regional and seasonal dimension. *Climatic Change*, **110**, 669–696, <https://doi.org/10.1007/s10584-011-0122-9>.
- Orsolini, Y., and Coauthors, 2019: Evaluation of snow depth and snow cover over the Tibetan Plateau in global reanalyses using in situ and satellite remote sensing observations. *Cryosphere*, **13**, 2221–2239, <https://doi.org/10.5194/tc-13-2221-2019>.
- Palazzi, E., J. Von Hardenberg, and A. Provenzale, 2013: Precipitation in the Hindu-Kush Karakoram Himalaya: Observations and future scenarios. *J. Geophys. Res. Atmos.*, **118**, 85–100, <https://doi.org/10.1029/2012JD018697>.
- Peng, D., T. Zhou, L. Zhang, and L. Zou, 2019: Detecting human influence on the temperature changes in central Asia. *Climate Dyn.*, **53**, 4553–4568, <https://doi.org/10.1007/s00382-019-04804-2>.
- Pepin, N., and Coauthors, 2015: Elevation-dependent warming in mountain regions of the world. *Nat. Climate Change*, **5**, 424–430, <https://doi.org/10.1038/nclimate2563>.
- Puma, M. J., and B. I. Cook, 2010: Effects of irrigation on global climate during the 20th century. *J. Geophys. Res.*, **115**, D16120, <https://doi.org/10.1029/2010JD014122>.
- Qin, J., K. Yang, S. Liang, and X. Guo, 2009: The altitudinal dependence of recent rapid warming over the Tibetan Plateau. *Climatic Change*, **97**, 321, <https://doi.org/10.1007/s10584-009-9733-9>.
- Qin, Y., and Coauthors, 2020: Agricultural risks from changing snowmelt. *Nat. Climate Change*, **10**, 459–465, <https://doi.org/10.1038/s41558-020-0746-8>.
- Qutbudin, I., M. S. Shiru, A. Sharafati, K. Ahmed, N. Al-Ansari, Z. M. Yaseen, S. Shahid, and X. Wang, 2019: Seasonal drought pattern changes due to climate variability: Case study in Afghanistan. *Water*, **11**, 1096, <https://doi.org/10.3390/w11051096>.
- Ramanathan, V., and G. Carmichael, 2008: Global and regional climate changes due to black carbon. *Nat. Geosci.*, **1**, 221–227, <https://doi.org/10.1038/ngeo156>.
- Raymond, C., T. Matthews, and R. M. Horton, 2020: The emergence of heat and humidity too severe for human tolerance. *Sci. Adv.*, **6**, eaaw1838, <https://doi.org/10.1126/sciadv.aaw1838>.
- Rees, H. G., and D. N. Collins, 2006: Regional differences in response of flow in glacier-fed Himalayan rivers to climatic warming. *Hydrol. Processes*, **20**, 2157–2169, <https://doi.org/10.1002/hyp.6209>.
- Ren, Y.-Y., and Coauthors, 2017: Observed changes in surface air temperature and precipitation in the Hindu Kush Himalayan region over the last 100-plus years. *Adv. Climate Change Res.*, **8**, 148–156, <https://doi.org/10.1016/j.accre.2017.08.001>.
- Roy, N. S., and S. Kaur, 2000: Climatology of monsoon rains of Myanmar (Burma). *Int. J. Climatol.*, **20**, 913–928, [https://doi.org/10.1002/1097-0088\(20000630\)20:8<913::AID-JOC485>3.0.CO;2-U](https://doi.org/10.1002/1097-0088(20000630)20:8<913::AID-JOC485>3.0.CO;2-U).
- Saha, A., and S. Ghosh, 2019: Can the weakening of Indian monsoon be attributed to anthropogenic aerosols? *Environ. Res. Commun.*, **1**, 061006, <https://doi.org/10.1088/2515-7620/ab2c65>.
- , —, A. S. Sahana, and E. P. Rao, 2014: Failure of CMIP5 climate models in simulating post-1950 decreasing trend of Indian monsoon. *Geophys. Res. Lett.*, **41**, 7323–7330, <https://doi.org/10.1002/2014GL061573>.
- Salama, M. S., R. van der Velde, L. Zhong, Y. Ma, M. Ofwono, and Z. Su, 2012: Decadal variations of land surface temperature anomalies observed over the Tibetan Plateau by the special sensor microwave imager (SSM/I) from 1987 to 2008. *Climatic Change*, **114**, 769–781, <https://doi.org/10.1007/s10584-012-0427-3>.
- Salerno, F., and Coauthors, 2015: Weak precipitation, warm winters and springs impact glaciers of south slopes of Mt. Everest (central Himalaya) in the last 2 decades (1994–2013). *Cryosphere*, **9**, 1229–1247, <https://doi.org/10.5194/tc-9-1229-2015>.
- Schiemann, R., D. Lüthi, and C. Schär, 2009: Seasonality and interannual variability of the westerley jet in the Tibetan Plateau region. *J. Climate*, **22**, 2940–2957, <https://doi.org/10.1175/2008JCLI2625.1>.
- Sen, P. K., 1968: Estimates of the regression coefficient based on Kendall's Tau. *J. Amer. Stat. Assoc.*, **63**, 1379–1389, <https://doi.org/10.1080/01621459.1968.10480934>.
- Shean, D. E., S. Bhushan, P. Montesano, D. R. Rounce, A. Arendt, and B. Osmanoglu, 2020: A systematic, regional assessment of High Mountain Asia glacier mass balance. *Front. Earth Sci.*, **7**, 363, <https://doi.org/10.3389/feart.2019.00363>.
- Shi, J., L. Cui, K. Wen, Z. Tian, P. Wei, and B. Zhang, 2018: Trends in the consecutive days of temperature and precipitation extremes in China during 1961–2015. *Environ. Res.*, **161**, 381–391, <https://doi.org/10.1016/j.envres.2017.11.037>.
- Shinoda, M., 2001: Climate memory of snow mass as soil moisture over central Eurasia. *J. Geophys. Res.*, **106**, 33 393–33 403, <https://doi.org/10.1029/2001JD000525>.
- Shrestha, A. B., C. P. Wake, P. A. Mayewski, and J. E. Dibb, 1999: Maximum temperature trends in the Himalaya and its vicinity: An analysis based on temperature records from Nepal for the period 1971–94. *J. Climate*, **12**, 2775–2786, [https://doi.org/10.1175/1520-0442\(1999\)012<2775:MTTITH>2.0.CO;2](https://doi.org/10.1175/1520-0442(1999)012<2775:MTTITH>2.0.CO;2).
- , —, J. E. Dibb, and P. A. Mayewski, 2000: Precipitation fluctuations in the Nepal Himalaya and its vicinity and

- relationship with some large scale climatological parameters. *Int. J. Climatol.*, **20**, 317–327, [https://doi.org/10.1002/\(SICI\)1097-0088\(20000315\)20:3<317::AID-JOC476>3.0.CO;2-G](https://doi.org/10.1002/(SICI)1097-0088(20000315)20:3<317::AID-JOC476>3.0.CO;2-G).
- Sigdel, M., and Y. Ma, 2017: Variability and trends in daily precipitation extremes on the northern and southern slopes of the central Himalaya. *Theor. Appl. Climatol.*, **130**, 571–581, <https://doi.org/10.1007/s00704-016-1916-5>.
- Simmons, A. J., K. M. Willett, P. D. Jones, P. W. Thorne, and D. P. Dee, 2010: Low-frequency variations in surface atmospheric humidity, temperature, and precipitation: Inferences from reanalyses and monthly gridded observational data sets. *J. Geophys. Res.*, **115**, D01110, <https://doi.org/10.1029/2009JD012442>.
- Song, C., Y. Sheng, J. Wang, L. Ke, A. Madson, and Y. Nie, 2017: Heterogeneous glacial lake changes and links of lake expansions to the rapid thinning of adjacent glacier termini in the Himalayas. *Geomorphology*, **280**, 30–38, <https://doi.org/10.1016/j.geomorph.2016.12.002>.
- Su, F., X. Duan, D. Chen, Z. Hao, and L. Cuo, 2013: Evaluation of the global climate models in the CMIP5 over the Tibetan Plateau. *J. Climate*, **26**, 3187–3208, <https://doi.org/10.1175/JCLI-D-12-00321.1>.
- Sun, H., and Coauthors, 2021: General overestimation of ERA5 precipitation in flow simulations for High Mountain Asia basins. *Environ. Res. Commun.*, **3**, 121003, <https://doi.org/10.1088/2515-7620/ac40f0>.
- Svoboda, M., and B. Fuchs, 2017: *Handbook of Drought Indicators and Indices*. CRC Press, 155 pp.
- Tang, G., M. P. Clark, S. M. Papalexiou, Z. Ma, and Y. Hong, 2020: Have satellite precipitation products improved over last two decades? A comprehensive comparison of GPM IMERG with nine satellite and reanalysis datasets. *Remote Sens. Environ.*, **240**, 111697, <https://doi.org/10.1016/j.rse.2020.111697>.
- Thiery, W., E. L. Davin, D. M. Lawrence, A. L. Hirsch, M. Hauser, and S. I. Seneviratne, 2017: Present-day irrigation mitigates heat extremes. *J. Geophys. Res. Atmos.*, **122**, 1403–1422, <https://doi.org/10.1002/2016JD025740>.
- Thorne, P. W., and R. S. Vose, 2010: Reanalyses suitable for characterizing long-term trends. *Bull. Amer. Meteor. Soc.*, **91**, 353–362, <https://doi.org/10.1175/2009BAMS2858.1>.
- Tong, K., F. Su, D. Yang, L. Zhang, and Z. Hao, 2014: Tibetan Plateau precipitation as depicted by gauge observations, reanalyses and satellite retrievals. *Int. J. Climatol.*, **34**, 265–285, <https://doi.org/10.1002/joc.3682>.
- Veh, G., O. Korup, and A. Walz, 2020: Hazard from Himalayan glacier lake outburst floods. *Proc. Natl. Acad. Sci. USA*, **117**, 907–912, <https://doi.org/10.1073/pnas.1914898117>.
- Wang, L., and Coauthors, 2022: Observing multisphere hydrological changes in the largest River Basin of the Tibetan Plateau. *Bull. Amer. Meteor. Soc.*, **103**, E1595–E1620, <https://doi.org/10.1175/BAMS-D-21-0217.1>.
- Wang, X., V. Tolksdorf, M. Otto, and D. Scherer, 2020: WRF-based dynamical downscaling of ERA5 reanalysis data for High Mountain Asia: Towards a new version of the High Asia refined analysis. *Int. J. Climatol.*, **41**, 743–762, <https://doi.org/10.1002/joc.6686>.
- Webster, P. J., V. O. Magaña, T. N. Palmer, J. Shukla, R. A. Tomas, M. Yanai, and T. Yasunari, 1998: Monsoons: Processes, predictability, and the prospects for prediction. *J. Geophys. Res.*, **103**, 14451–14510, <https://doi.org/10.1029/97JC02719>.
- Wijngaard, R. R., A. F. Lutz, S. Nepal, S. Khanal, S. Pradhananga, A. B. Shrestha, and W. W. Immerzeel, 2017: Future changes in hydro-climatic extremes in the Upper Indus, Ganges, and Brahmaputra River basins. *PLOS ONE*, **12**, e0190224, <https://doi.org/10.1371/journal.pone.0190224>.
- Xu, M., S. Kang, H. Wu, and X. Yuan, 2018: Detection of spatio-temporal variability of air temperature and precipitation based on long-term meteorological station observations over Tianshan Mountains, central Asia. *Atmos. Res.*, **203**, 141–163, <https://doi.org/10.1016/j.atmosres.2017.12.007>.
- Xu, Z., Z. Liu, G. Fu, and Y. Chen, 2010: Trends of major hydro-climatic variables in the Tarim River basin during the past 50 years. *J. Arid Environ.*, **74**, 256–267, <https://doi.org/10.1016/j.jaridenv.2009.08.014>.
- Yan, L., and X. Liu, 2014: Has climatic warming over the Tibetan Plateau paused or continued in recent years. *J. Earth Ocean Atmos. Sci.*, **1**, 13–28.
- Yang, K., B. Ye, D. Zhou, B. Wu, T. Foken, J. Qin, and Z. Zhou, 2011: Response of hydrological cycle to recent climate changes in the Tibetan Plateau. *Climatic Change*, **109**, 517–534, <https://doi.org/10.1007/s10584-011-0099-4>.
- , H. Wu, J. Qin, C. Lin, W. Tang, and Y. Chen, 2014: Recent climate changes over the Tibetan Plateau and their impacts on energy and water cycle: A review. *Global Planet. Change*, **112**, 79–91, <https://doi.org/10.1016/j.gloplacha.2013.12.001>.
- Yang, M., F. E. Nelson, N. I. Shiklomanov, D. Guo, and G. Wan, 2010: Permafrost degradation and its environmental effects on the Tibetan Plateau: A review of recent research. *Earth-Sci. Rev.*, **103**, 31–44, <https://doi.org/10.1016/j.earscirev.2010.07.002>.
- Yao, T., and Coauthors, 2012: Third pole environment (TPE). *Environ. Dev.*, **3**, 52–64, <https://doi.org/10.1016/j.envdev.2012.04.002>.
- Yatagai, A., K. Kamiguchi, O. Arakawa, A. Hamada, N. Yasutomi, and A. Kitoh, 2012: APHRODITE constructing a long-term daily gridded precipitation dataset for Asia based on a dense network of rain gauges. *Bull. Amer. Meteor. Soc.*, **93**, 1401–1415, <https://doi.org/10.1175/BAMS-D-11-00122.1>.
- You, Q., S. Kang, E. Aguilar, and Y. Yan, 2008: Changes in daily climate extremes in the eastern and central Tibetan Plateau during 1961–2005. *J. Geophys. Res.*, **113**, D07101, <https://doi.org/10.1029/2007JD009389>.
- , J. Min, W. Zhang, N. Pepin, and S. Kang, 2015a: Comparison of multiple datasets with gridded precipitation observations over the Tibetan Plateau. *Climate Dyn.*, **45**, 791–806, <https://doi.org/10.1007/s00382-014-2310-6>.
- , —, H. Lin, N. Pepin, M. Sillanpää, and S. Kang, 2015b: Observed climatology and trend in relative humidity in the central and eastern Tibetan Plateau. *J. Geophys. Res. Atmos.*, **120**, 3610–3621, <https://doi.org/10.1002/2014JD023031>.
- , G.-Y. Ren, Y.-Q. Zhang, Y.-Y. Ren, X.-B. Sun, Y.-J. Zhan, A. B. Shrestha, and R. Krishnan, 2017: An overview of studies of observed climate change in the Hindu Kush Himalayan (HKH) region. *Adv. Climate Change Res.*, **8**, 141–147, <https://doi.org/10.1016/j.accre.2017.04.001>.
- Yu, X., L. Zhang, T. Zhou, and J. Liu, 2021: The Asian subtropical westerly jet stream in CRA-40, ERA5, and CFSR reanalysis data: Comparative assessment. *J. Meteor. Res.*, **35**, 46–63, <https://doi.org/10.1007/s13351-021-0107-1>.
- Yue, S., and C. Y. Wang, 2002: Applicability of prewhitening to eliminate the influence of serial correlation on the Mann–Kendall test. *Water Resour. Res.*, **38**, 1068, <https://doi.org/10.1029/2001WR000861>.
- Zandler, H., I. Haag, and C. Samimi, 2019: Evaluation needs and temporal performance differences of gridded precipitation

- products in peripheral mountain regions. *Sci. Rep.*, **9**, 15118, <https://doi.org/10.1038/s41598-019-51666-z>.
- Zhan, Y.-J., and Coauthors, 2017: Changes in extreme precipitation events over the Hindu Kush Himalayan region during 1961–2012. *Adv. Climate Change Res.*, **8**, 166–175, <https://doi.org/10.1016/j.accre.2017.08.002>.
- Zhang, C., Q. Tang, D. Chen, R. J. van der Ent, X. Liu, W. Li, and G. G. Haile, 2019: Moisture source changes contributed to different precipitation changes over the northern and southern Tibetan Plateau. *J. Hydrometeor.*, **20**, 217–229, <https://doi.org/10.1175/JHM-D-18-0094.1>.
- Zhang, G., T. Yao, H. Xie, W. Wang, and W. Yang, 2015: An inventory of glacial lakes in the third pole region and their changes in response to global warming. *Global Planet. Change*, **131**, 148–157, <https://doi.org/10.1016/j.gloplacha.2015.05.013>.
- Zhang, M., Y. Chen, Y. Shen, and B. Li, 2019: Tracking climate change in central Asia through temperature and precipitation extremes. *J. Geogr. Sci.*, **29**, 3–28, <https://doi.org/10.1007/s11442-019-1581-6>.
- Zhang, Q., Y. Pan, S. Wang, J. Xu, and J. Tang, 2017: High-resolution regional reanalysis in China: Evaluation of 1 year period experiments. *J. Geophys. Res. Atmos.*, **122**, 10801–10819, <https://doi.org/10.1002/2017JD027476>.
- Zhang, X., L. Alexander, G. C. Hegerl, P. Jones, A. K. Tank, T. C. Peterson, B. Trewin, and F. W. Zwiers, 2011: Indices for monitoring changes in extremes based on daily temperature and precipitation data. *Wiley Interdiscip. Rev.: Climate Change*, **2**, 851–870, <https://doi.org/10.1002/wcc.147>.
- Zhao, P., S. Yang, and R. Yu, 2010: Long-term changes in rainfall over eastern China and large-scale atmospheric circulation associated with recent global warming. *J. Climate*, **23**, 1544–1562, <https://doi.org/10.1175/2009JCLI2660.1>.
- Zhong, L., Z. Su, Y. Ma, M. S. Salama, and J. A. Sobrino, 2011: Accelerated changes of environmental conditions on the Tibetan Plateau caused by climate change. *J. Climate*, **24**, 6540–6550, <https://doi.org/10.1175/JCLI-D-10-05000.1>.
- , Y. Ma, Y. Xue, and S. Piao, 2019: Climate change trends and impacts on vegetation greening over the Tibetan Plateau. *J. Geophys. Res. Atmos.*, **124**, 7540–7552, <https://doi.org/10.1029/2019JD030481>.
- Zhou, B., Q. H. Wen, Y. Xu, L. Song, and X. Zhang, 2014: Projected changes in temperature and precipitation extremes in China by the CMIP5 multimodel ensembles. *J. Climate*, **27**, 6591–6611, <https://doi.org/10.1175/JCLI-D-13-00761.1>.
- Zhu, Y., Y. F. Sang, D. Chen, B. Sivakumar, and D. Li, 2020: Effects of the South Asian summer monsoon anomaly on interannual variations in precipitation over the south-central Tibetan Plateau. *Environ. Res. Lett.*, **15**, 124067, <https://doi.org/10.1088/1748-9326/abc71b>.